GREEN SYNTHESIS OF IRON OXIDE NANOPARTICLES USING *Citrus maxima* PEEL EXTRACT, ITS CHARACTERIZATION AND STUDY OF THEIR ANTIMICROBIAL AND PHOTOCATALYTIC ACTIVITY

A DISSERTATION SUBMITTED FOR THE PARTIAL FULFILLMENT OF THE REQUIREMENTS FOR THE MASTER OF SCIENCE DEGREE IN CHEMISTRY

BY

BIJAY KUMAR DAS

Exam Symbol No: 1872 / 076

TU Regd. No: 5-3-33-406-2019

AMRIT CAMPUS

DEPARTMENT OF CHEMISTRY

INSTITUTE OF SCIENCE AND TECHNOLOGY

TRIBHUVAN UNIVERSITY

KATHMANDU, NEPAL

December 21, 2023

BOARD OF EXAMINERS AND CERTIFICATE OF APPROVAL

This dissertation entitled, **"Green Synthesis of Iron Oxide Nanoparticles Using *Citrus maxima* Peel Extract, Its Characterization and Study of Their Antimicrobial and Photocatalytic Activity"** by Bijay Kumar Das under the supervision of Asst. Prof. Dr. Kamal Prasad Sapkota, Department of Chemistry, Amrit Campus, Tribhuvan University, Kathmandu, has been accepted for the partial fulfillment of the Master of Science (M. Sc.) Degree in Chemistry.

Supervisor

Asst. Prof. Dr. Kamal Prasad Sapkota

Department of Chemistry, Amrit Campus

Tribhuvan University, Kathmandu, Nepal

Internal Examiner

Assoc. Prof. Dr. Sharmila Pradhan

Department of Chemistry

Amrit Campus

Tribhuvan University

Lainchaur, Kathmandu, Nepal

External Examiner

Prof. Dr. Megh Raj Pokhrel

Central Department of Chemistry

Tribhuvan University

Kirtipur, Kathmandu, Nepal

M. Sc. Chemistry Coordinator

Assoc. Prof. Dr. Bhushan Shakya

Department of Chemistry

Amrit Campus

Tribhuvan University

Lainchaur, Kathmandu, Nepal

Head of the Department

Assoc. Prof. Kanchan Sharma

Department of Chemistry

Amrit Campus

Tribhuvan University

Lainchaur, Kathmandu, Nepal

Date: 21-12-2023

RECOMMENDATION LETTER

This is to certify that this dissertation entitled, **"Green Synthesis of Iron Oxide Nanoparticles Using *Citrus maxima* Peel Extract, Its Characterization and Study of Their Antimicrobial and Photocatalytic Activity"** has been carried out by Bijay Kumar Das under my supervision. This thesis work was performed for the partial fulfillment of the Master of Science in Chemistry under the course of code (CHE-654). To the best of my knowledge, this dissertation work has not been submitted for any other degree at this institute. I recommend this dissertation for the final evaluation.

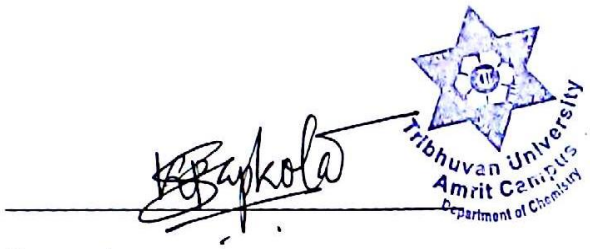

Supervisor

Asst. Prof. Dr. Kamal Prasad Sapkota

Department of Chemistry, Amrit Campus

Tribhuvan University

Kathmandu, Nepal

Date: 21-12-2023

DECLARATION

I, Bijay Kumar Das, hereby declare that the dissertation entitled, **"Green Synthesis of Iron Oxide Nanoparticles Using *Citrus maxima* Peel Extract, Its Characterization and Study of Their Antimicrobial and Photocatalytic Activity"** is a research work done by me under the supervision of Asst. Prof. Dr. Kamal Prasad Sapkota. This research work has not been previously submitted for the award of any degree, diploma, associateship, fellowship or any other similar titles of any other university or society. Also, I declare that the submitted work represents my original ideas in my own words. In case other's ideas or words have been included, I have adequately cited and duly referenced the sources.

Bijay.

Bijay Kumar Das

Department of Chemistry

Amrit Campus

Tribhuvan University

Lainchaur, Kathmandu

Date: 21-12-2023

ACKNOWLEDGEMENTS

I am greatly honored to express profound gratitude to my respected supervisor **Asst. Prof. Dr. Kamal Prasad Sapkota**, Department of Chemistry, Amrit Campus, Tribhuvan University for offering me valuable advice, encouragement, guidance and skillful knowledge that helped me throughout this dissertation work. My special gratitude goes to the Amrit Campus, Department of Chemistry for providing me the platform to carry out my research work within the department successfully.

I am also thankful to **Assoc. Prof. Dr. Bhushan Shakya,** Co-ordinator of M.Sc. Chemistry for his humility for being a constant source of motivation to students committed to research. I am grateful to the Department of Chemistry for providing the chemicals, instruments and other physical facilities for the execution of this research. I am grateful to the **Assoc. Prof. Kanchan Sharma,** Head of the Department, Department of Chemistry, Amrit Campus. I am equally grateful to all the professors of the Department of Chemistry for their advice and support.

I am greatly thankful to the Nepal Academy of Science and Technology (NAST), Khumaltar, Lalitpur, Nepal for their valuable help with sample characterization involving XRD analysis of the sample. I am equally thankful to the Himalaya Research Institute of Biotechnology Pvt. Ltd., Srijananagar, Bhaktapur, Nepal for their valuable help for carrying out the investigation of anti-microbial activity of synthesized iron oxide nanoparticles.

I am especially indebted to my parents for their continuous support, patience, and incessant encouragement that led towards successful completion of my formal study. I am very thankful to all my friends for their help during the thesis work. I am grateful to all the faculty members and non-teaching staffs of Amrit Campus who supported me directly or indirectly during this work.

.....Bijay.....

Bijay Kumar Das

December 21, 2023

ABSTRACT

The iron oxide nanoparticles possess unique fascinating properties such as stability in chemical environments, high thermal and electrical conductivity, distinct optical characteristics and a powerful ability to combine with biomolecules. The preference for green synthesis is growing as it provides an alternative, eco-friendly, cost-effective and convenient method of producing nanoparticles using plants and other biological systems. The synthesized nanoparticles were characterized by using UV-visible spectroscopy, Fourier Transform Infra-red Spectroscopy (FTIR) and X-ray Diffraction (XRD) techniques. The nanoparticles were then employed for the photocatalytic degradation of methylene blue (MB) under sunlight with monitoring using a UV-visible spectrophotometer. The results confirmed the synthesis of iron oxide nanoparticles (IONPs) through observed color changes and further characterization using UV-visible spectroscopy, Fourier Transform Infra-red Spectroscopy (FTIR) and X-ray Diffraction (XRD) techniques. The maximum absorption peak at 353 nm indicated a crystalline structure with an average size of 8.70 nm as determined by XRD analysis. In conclusion, the extract from *C.maxima* peel extract demonstrated great potential as a reducing and stabilizing agent for the biosynthesis of iron oxide nanoparticles. These nanoparticles can be effectively utilized for the photocatalytic degradation of methylene blue in industrial wastewater and other polluted water streams as well as for antimicrobial applications.

Keywords: Green synthesis, Iron oxide nanoparticles, UV-visible spectroscopy, FTIR, XRD, Phytochemical analysis, Photocatalytic degradation, Anti-microbial activity.

शोधसार

Iron oxide nanoparticles सँग अद्वितीय आकर्षक गुणहरू छन् जस्तै रसायनिक वातावरणमा स्थिरता, उच्च थर्मल र विधुतीय चालकता, विशिष्ट अप्टिकल विशेषताहरू र बायोमोलिक्युलहरूसँग संयोजन गर्ने शक्तिशाली क्षमता। Green synthesis को प्राथमिकता बढ्दै गएको छ किनकि यसले बिरुवा र अन्य जैविक प्रणालीहरू प्रयोग गरेर nanoparticles उत्पादन गर्न वैकल्पिक, पर्यावरण मैत्री, लागत प्रभावी र सुविधाजनक विधि प्रदान गर्दछ।बनेको IONPs हरुको characterization UV-visible spectroscopy, Fourier Transform Infra-red Spectroscopy (FTIR) र X-ray Diffraction (XRD) प्रविधिहरू प्रयोग गरेर पुष्टि गरिएको थियो। IONPs बनेको पुष्टी रंग बदलेको र UV-visible spectroscopy मार्फत 353 nm मा maximum absorption peak को संकेत गऱ्यो।साथै 8.70 nm को औसत आकारको क्रिस्टल संरचना XRD विश्लेषण मार्फत निर्धारण गरिएको थियो। त्यसपछि IONPs लाई प्राकृतिक सूर्यको प्रकाश अन्तर्गत Methylene blue (MB) को photocatalytic degradation को लागि प्रयोग गऱ्यो र यसको dye degradation मा परिवर्तनको निगरानी UV-visible spectroscopy को प्रयोग द्वारा गऱ्यो । तसर्थ, C. *maxima* peel extract को प्रयोगले iron oxide nanoparticles (IONPs) biosynthesis को लागि reducing र stabilizing गर्ने एजेन्टको रूपमा ठूलो सम्भावना देखाएको छ र औद्योगिक फोहोर पानी र अन्य प्रदूषित पानीका स्रोतहरुमा methylene blue photo-degradation र anti-microbial applications हरूको लागि IONPs लाई प्रभावकारी रूपमा प्रयोग गर्न सकिन्छ भन्ने अनुमान गरिन्छ।

शब्दकुञ्जी: Green synthesis, Iron oxide nanoparticles, UV-visible spectroscopy, FTIR, XRD, phytochemical analysis, photocatalytic degradation, anti-microbial activity.

LIST OF ACRONYMS AND ABBREVIATIONS

IONPs	Iron Oxide Nanoparticles
UV-vis	Ultraviolet-visible
XRD	X-ray Diffraction
SEM	Scanning Electron Microscopy
TEM	Transmission Electron Microscopy
DLS	Dynamic Light Scattering
AFM	Atomic Force Microscopy
FTIR	Fourier Transform Infrared Spectroscopy
TGA	Thermogravimetric Analysis
MRI	Magnetic Resonance Imaging
FE-SEM	Field Emission Scanning Electron Microscopy
HR-TEM	High-resolution Transmission Electron Microscopy
EDX/EDS	Energy Dispersive X-ray Spectroscopy
XPS	X-ray Photoelectron Spectroscopy
FWHM	Full Width at Half Maximum
LSPR	Local Surface Plasmon Resonance
MB	Methylene Blue
DNA	Deoxyribonucleic Acid
ZOI	Zone of Inhibition
PPM	Parts Per Million

LIST OF TABLES

LIST OF FIGURES

TABLE OF CONTENTS

CHAPTER 1

1. INTRODUCTION

1.1 Nanotechnology

Nanotechnology is an emerging scientific field focused on synthesizing and assembling materials at the nanometer scale (1-100 nm). Metal nanoparticles known for their high specific surface area and large proportion of surface atoms have been extensively studied due to their unique physicochemical properties including electronic, magnetic, catalytic, optical, anti-corrosion, and antimicrobial activities. The field of nanotechnology is rapidly advancing and holds significant importance due to its continuous development and wide range of applications in catalysis, agriculture, electronics, biomedical analysis, and even groundwater purification (Naseem *et al.*, 2021).There are two approaches commonly used for nanoparticle synthesis; the top-down approach where a larger structure is broken down into smaller pieces using chemical, physical or biological energy and the bottom-up approach where materials are synthesized from the atomic level to form a larger nanostructure. Various physical and chemical methods have been employed for bottom-up synthesis such as chemical reduction, photochemical reduction, electrochemical reduction, heat-induced evaporation and biological techniques. In the biosynthesis of nanoparticles, a bottom-up approach primarily involves reduction or oxidation reactions. Recently, new methods utilizing biological sources like microorganisms, microbial extracts or products and plant extracts have been introduced to overcome the issues associated with conventional physical and chemical methods which often generate reactive and toxic residues that pollute the environment. Researchers are actively working on developing green chemistry processes that are facile, effective, sustainable, and reliable for nanomaterial production (Narayan *et al.*, 2019; Kumar *et al.*, 2020).

1.2 Classification of Nanoparticles

Nanoparticles can be categorized based on their dimensionality, morphology, composition, uniformity and agglomeration (Buzea *et al.*, 2007). According to Siegel, mono-structured materials can be classified dimensionally as follows:

I. Zero-dimensional nanoclusters
II. One-dimensional multilayers
III. Two-dimensional nano-grained layer

IV. Three-dimensional Equiaxed bulk solid

1.2.1 Zero-dimensional Nanomaterials (0-D)

Zero-dimensional nanoparticles exhibit a unique and uniform size encompassing all three axes (X, Y, and Z) at the nanoscale. Examples of such nanoparticles include quantum dots, metallic nanoclusters, nanocubes and nanospheres (Figure 1.1).

1.2.2 One-dimensional Nanomaterials (1-D)

One-dimensional nanomaterials possess nano-scale dimensions in two out of three dimensions while one dimension exceeds the nano-scale range. Nanorods, nanofibers, nanotubes and nanowires (Figure 1.1) are some examples of one-dimensional nanoparticles (Brown *et al.*, 2007).

1.2.3 Two-dimensional Nanomaterials (2-D)

Two-dimensional nanomaterials have one external dimension within the nanoscale range while the remaining dimensions lie beyond the nanoscopic range. Examples of such materials include nanofilms, nano-coatings and nano-plates (Figure 1.1) (Ohring, 2001).

1.2.4 Three-dimensional Nanomaterials (3-D)

Three-dimensional nanoparticles are characterized by having all external dimensions beyond the nano-scale range while displaying nano-scale properties internally. Nano-composites and nano-structured materials (Figure 1.1) serve as examples of three-dimensional nanomaterials (Camargo *et al.*, 2009).

1.3 Nanoparticle Morphology

In general, nanoparticles exhibit diverse morphological characteristics with factors such as flatness, sphericity and aspect ratio being extensively studied and considered. For instance, nanotubes and nanowires display different shapes such as helices, zigzags and belts, representing high aspect ratio nanoparticles. On the other hand, nanoparticles with small aspect ratios exhibit morphologies like spherical, oval, cubic, prism, and helical shapes (Buzea *et al.*, 2007).

1.4 Nanoparticle Composition

Nanoparticles consist of either a single material or a composite of multiple materials. In their natural state, nanoparticles exist as agglomerates with various compositions while single- composition materials can be formed without complex processes using a range of

procedures. Nanoparticles are classified based on their composition and several well-known types of nanoparticles fall into this category (Buzea *et al.*, 2007).

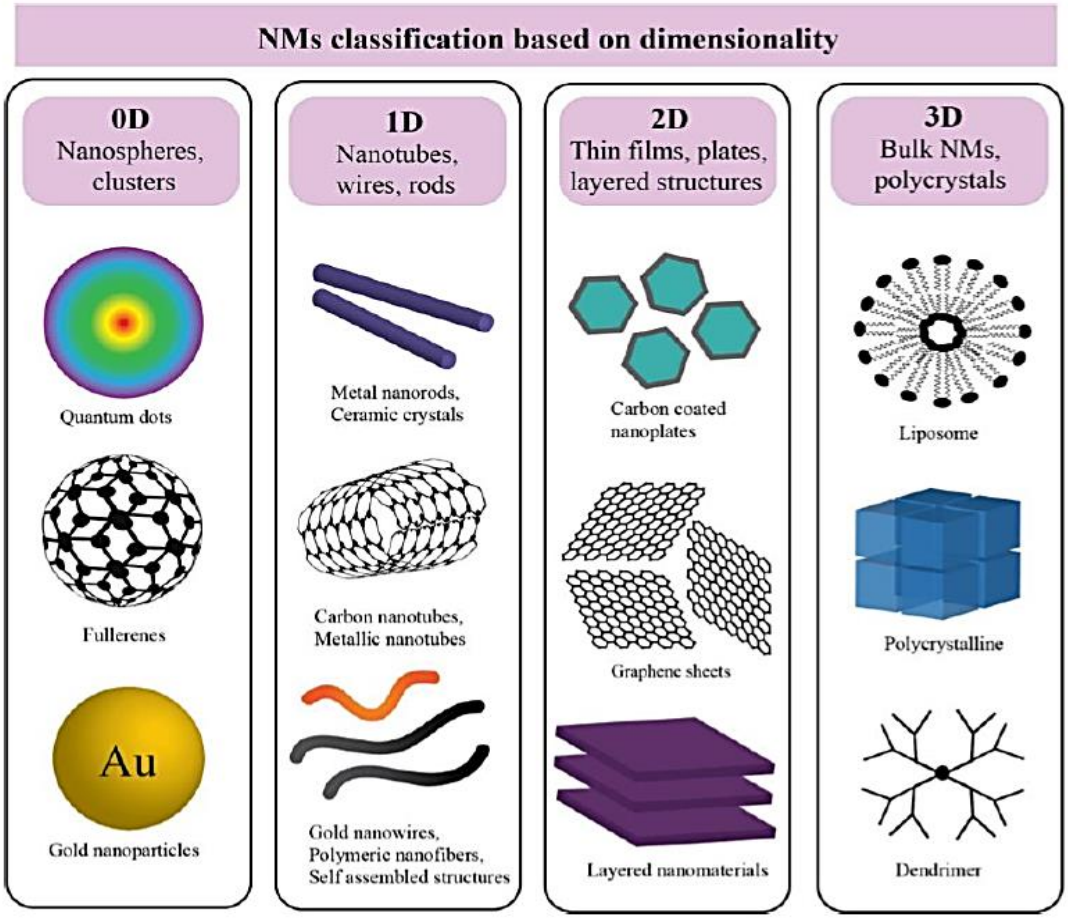

Figure 1.1: Schematic illustration of the relative dimension of nanoparticles with examples (Poh *et al.*, 2018).

1.4.1 Carbon-based Nanoparticles

Carbon-based nanoparticles encompass carbon nanotubes and fullerene. Fullerene refers to a globular hollow carbon nanotube which is also considered as carbon allotrope. It possesses significant applications in the commercial sector due to its electrical conductivity, structural rigidity, good electron affinity and diverse uses (Astefanei *et al.*, 2015).

Fullerenes are structured with pentagonal and hexagonal units with Sp^2 hybridized carbon atoms playing a crucial role in their formation. Notably, C_{60} and C_{70} are well-known fullerenes with diameters of 7.114 nm and 7.648 nm, respectively. Carbon nanotubes, on the other hand, are elongated and tubular with diameters ranging from 1 to 2 nm. They can exist as single-walled (SWNTs), double-walled (DWNTs) or multi-walled (MWNTs)

carbon nanotubes. Various processes are employed using atomic carbon vaporization through laser or electric arc on metal particles derived from graphite. Chemical vapor deposition (CVD) has also been recently utilized for the synthesis of carbon nanotubes (Elliott *et al.*, 2013).

1.4.2 Metal Nanoparticles

Metal nanoparticles are exclusively composed of metal precursors. They exhibit well-known localized surface plasmon resonance (LSPR) characteristics resulting in unique opto-electrical properties. Notably, alkali and noble metals such as Cu have absorption bands in the visible range of the solar electromagnetic spectrum. The precise control of surface smoothness, size and shape during the synthesis of nanoparticles is crucial for advanced materials. Metal nanoparticles find wide range of applications in various research areas due to their advanced optical properties. For instance, gold nanoparticles are commonly coated onto SEM samples to enhance electron conductivity, thereby improving the quality of SEM images. Additionally, Au nanoparticles efficiently convert absorbed light into localized heat making them suitable for selective laser photo-thermal therapy in cancer treatment (Jain *et al.*, 2007; Khandel *et al.*, 2018).

1.4.3 Ceramic Nanoparticles

Ceramic nanoparticles belong to the category of inorganic non-metallic nanoparticles and are synthesized through heat and subsequent cooling processes. They can have various morphologies including amorphous, polycrystalline, dense, porous or hollow structures. These nanoparticles find extensive applications in catalysis, photolysis, photo-degradation of organic dyes and imaging leading to increased research focus on them (Thomas et. al., 2015).

1.4.4 Semiconductor Nanoparticles

Semiconductor nanoparticles possess properties of both metals and non-metals making them highly versatile and widely studied. They exhibit wide band gaps which allows for significant property alterations through band gap tuning. Consequently, they play a crucial role in photocatalysis, photo optics and electronic devices. Their suitable band gap and band edge positions make them particularly useful in water-splitting applications (Hisatomi *et al.*, 2014).

1.4.5 Polymeric Nanoparticles

Polymeric nanoparticles often referred to as polymer nanoparticles (PNPs) are organic-based nanoparticles that primarily exist as nanospheres or nano capsules. PNPs are easily functionalized leading to their widespread applications in various fields (Abd Ellah *et al.*, 2017).

1.4.6 Lipid-based Nanoparticles

Lipid-based nanoparticles consist of lipid fragments and possess numerous biomedical applications. Morphologically, these nanoparticles are generally spherical with diameters ranging from 10 to 100 nm. They feature a solid core composed of lipids and a matrix containing soluble lipophilic molecules. Lipid-based nanotechnology is a specialized area of research that focuses on the synthesis and structure of lipid nanoparticles for applications such as drug delivery and targeted delivery within the human body (Puri *et al.*, 2009).

1.5 Synthetic Procedure of Nanoparticles

Nanoparticles can be synthesized using various methods which can be broadly classified into two major approaches:

I. Bottom-up approach
II. Top-down approach

These approaches further encompass different sub-classes based on the specific operation, reaction conditions and protocols employed (Wang *et al.*, 2004).

1.5.1 Top-down Synthesis of Nanoparticles

The top-down synthesis method involves a destructive approach where a larger molecule serves as the precursor. This precursor molecule is then decomposed into individual units which are subsequently transformed into the desired nanoparticles. Grinding/milling, chemical vapor deposition (CVD), physical vapor deposition (PVD) and other decomposition techniques are commonly employed in this method (Figure 1.2). As an example, coconut shell (CS) nanoparticles can be synthesized using this approach. The raw CS powder is finely milled at different time intervals using a planetary mill and ceramic balls followed by the milling process throughout the entire nanoparticle synthesis.

According to a study, small spherical magnetic nanoparticles were synthesized using a top-down destructive approach from natural iron oxide (Fe_2O_3) ore. The particle size of

these nanoparticles ranged approximately from 20 to 50 nm. The synthesis process involved the presence of organic oleic acid (Priyadarshana *et al.*, 2016). In another study, colloidal carbon spherical particles with controlled sizes were synthesized using a simple top-down approach. The synthetic technique primarily relied on the continuous chemical adsorption of polyoxometalates (POM) on the carbon interfacial surface. This led to the formation of relatively fine spherical particles with high dispersion capacity and narrow size distribution from the initial black carbon aggregates through the adsorption process (Garrigue *et al.*, 2004).

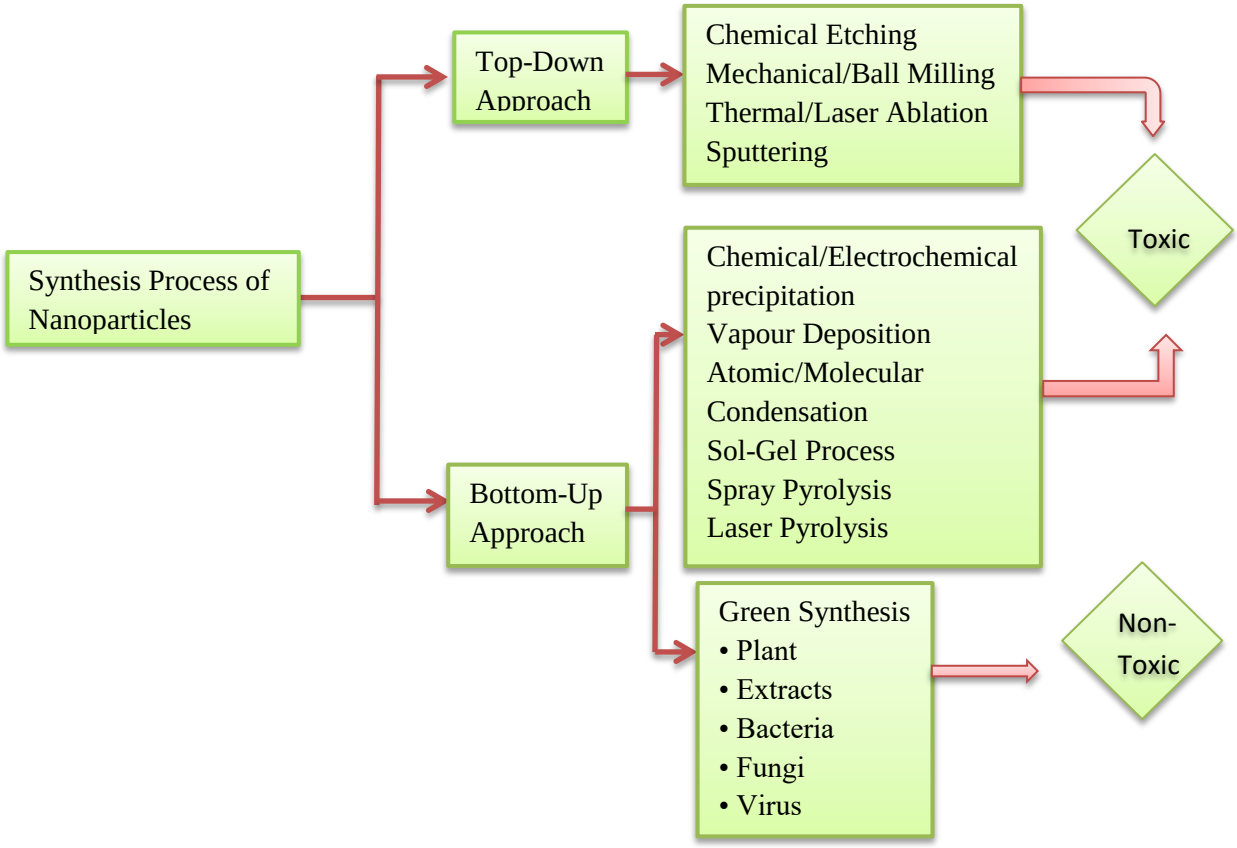

Figure 1.2: Schematic structure of bottom-up and top-down approach of iron oxide nanoparticle synthesis.

1.5.2 Bottom-up Synthesis of Nanoparticles

The bottom-up synthesis of nanoparticles involves the construction of nanoparticles from smaller components. Hence, it is often referred to as the "Building" approach. This method encompasses various techniques such as sedimentation, reduction, green synthesis, sol-gel, spinning, and biochemical synthesis (Figure 1.2). For instance, TiO_2 anatase nanoparticles were synthesized using the bottom-up approach incorporating a graphene domain. In the synthesis of a photoactive composite for the photocatalytic degradation of methylene blue, alizarin and titanium isopropoxide precursor were

utilized. It is note-worthy that alizarin possesses strong binding capacity with TiO_2 due to their axial hydroxyl terminal groups. The characterization of anatase was accomplished through X-ray diffraction (XRD) pattern analysis. The results indicated that the size of the nanoparticles increases as the temperature is raised. By employing a laser irradiation top-down technique, uniformly spherical Au nanospheres with a monocrystalline structure were selectively synthesized. Furthermore, the laser treatment time and other reaction parameters were controlled to convert the nanoparticles from an octahedral morphology to a spherical shape (Ahmed et. al., 2016).

1.6 Green Synthesis and Biogenic Bottom-up Synthesis of Nanoparticles

Green synthesis and biogenic bottom-up synthesis of nanoparticles are considered environmentally friendly approaches since they do not involve the use of toxic agents (Bibi *et al.*, 2019). Plants known as nature's "chemical factories", contain a vast array of secondary metabolites that can serve as redox mediators and stabilizers for nanoparticles. It has been reported that nanoparticles synthesized using plant products or extracts exhibit higher stability and easier synthesis rates compared to conventional techniques. Green approaches are considered eco-benign, cost-effective, simple and free from toxic agents (Wei *et al.*, 2016). To date, various metal and metal oxide nanoparticles have been successfully prepared using green routes and have found applications in different fields. Green synthesis of nanomaterials has gained importance due to its low cost, simplicity, availability, eco-friendliness, non-toxicity, and scalability. Moreover, green synthesis eliminates the need for multiple steps, high energy, high temperature, pressure, high chemical concentration and the use of toxic chemicals thus minimizing the formation of hazardous by-products and reducing costs. In this context, bio-resources such as plants, bacteria, fungi, algae, yeast and viruses have been explored as valuable and environmentally friendly precursors for the preparation of small-sized and stable nanoparticles (Adhikari *et al.*, 2022; Kumar *et al.*, 2020). The use of biomaterials as replacements for hazardous substances is a note-worthy approach in green nanotechnology. Utilizing different parts of plants for the synthesis of metal nanoparticles is the simplest and most cost-effective approach. Several studies have been conducted on the green synthesis of metal-based nanoparticles using various plant parts including fruit extracts of *Cucurbita maxima*, *Cynometra ramiflora*, rind of *Persea americana*, seed extracts of *Punica granatum*, flower extract of *Avicennia marina*, peel extracts of

Cucurbita maxima, Camellia sinensis, Citrus limon, leaf extract of *Cucurbita maxima, Psidium guajava, Carica papaya* as well as cell cultures of fungi, algae, and bacterial strains. Green synthesis of nanoparticles utilizes plant extracts as both reducing and capping agents eliminating the need for harmful reducing agents such as sodium borohydride, hydrogen peroxide, hydrazine and dimethylhydrazine which can have detrimental effects in various applications. Plant extracts contain various phytochemicals or secondary metabolites such as polyphenols, flavonoids, terpenoids, tannins, amides, aldehydes, ketones, phenolic acids, hydroxyl and carboxylic groups, citric acid, ascorbic acid, reducing sugars, reductases dehydrogenases, and extracellular electron shuttlers present in microbial enzymes. These compounds act as reducing and capping agents facilitating the reduction of metal precursors and the formation of stabilized metal nanoparticles (Izadiyan *et al.*, 2020).

1.7 Iron Oxide Nanoparticles

Various metals such as Cu, Ag, Ti, Zn, Al, Fe, Se, Si, and Mg are utilized in the synthesis of nanomaterials due to their distinct optical properties, high stability, and ability to conjugate with biomolecules. These nanomaterials have gained significant attention in nanotechnology for applications in industries such as textiles, catalysis, sensing, optics, antibacterial activity, and data storage. Gold, silver, copper, iron, zinc, and other metal nanoparticles are specifically employed in food packaging, wound dressings, catheters for drug delivery and other products due to their broad spectrum of antibacterial activities. Iron oxide nanoparticles (IONPs) occur naturally in the environment as particulate matter in air pollution and volcanic eruptions. They can also be chemically synthesized for various applications. The magnetic behavior of super paramagnetic IONPs plays a crucial role in their design and synthesis to maximize their potential applications. It is important to fabricate these nanoparticles using environmentally friendly techniques and biogenically synthesized IONPs can be equally employed in electronics, biomedical fields, material science and environmental remediation.

Different forms of iron oxide nanoparticles including Hematite (α-Fe_2O_3), Maghemite (γ-Fe_2O_3) and magnetite (Fe_3O_4) have been extensively studied. Various synthesis techniques such as sol-gel, chemical reduction, co-precipitation, hydrothermal synthesis, micro-emulsion, thermal decomposition, sono-chemical method, chemical vapor deposition (CVD), flow injection, electro-chemical techniques and laser-induced pyrolysis have been developed for IONPs synthesis. Hematite, maghemite and magnetite

are the most commonly studied iron oxides (Deraz *et al.*, 2013). Hematite is stable and possesses anti-ferromagnetic properties making it useful in gas sensors, pigments and catalysts which have gained attention for technological and scientific applications. Hematite can absorb visible light and serves as a cost-effective semiconductor and photocatalyst, while maghemite and magnetite are primarily employed in drug delivery, energy storage and data storage (Samrot *et al.*, 2018). Synthesis strategies such as sol-gel. chemical vapor deposition and pyrolysis often involve unsafe solvents and high pressures and temperatures which can affect the magnetic properties of iron-based nanoparticles. Chemical synthesis tends to result in oxidation of the iron-based nanomaterials leading to a loss of their magnetic properties.

Among various metal nanoparticles, iron and iron oxide nanoparticles have shown great potential in industrial and biomedical applications. Each of the three iron oxides mentioned possesses unique magnetic, catalytic, biochemical, and other properties suitable for specific biomedical and technical applications. While chemical and physical methods are commonly used for the synthesis of iron and iron oxide nanoparticles, various green and cost-effective synthesis methods have been developed (Deraz *et al.*, 2013). Protocols have also been expanded to include plants and other biological systems for nanoparticle synthesis. In our study, we employed a greener approach using a bottom-up method where nanostructures were synthesized by stacking atoms together resulting in uniformly distributed spherical iron oxide nanoparticles (IONPs).

1.7.1 Important Applications of Iron Oxide Nanoparticles

Iron oxide nanoparticles have found various applications in drug delivery, immune-purification, catalysis, MRI, hyperthermia, toxic-component mitigation and biocompatibility. The use of polymeric encapsulation or coating of iron oxide NPs improves their stability in water and allows for the design of smart or hybrid particles that can be used for targeted delivery of therapeutic agents. Additionally, the shape and size tuning of these particles plays a role in their pharmacokinetics, bio-distribution and immune clearance (Ali *et al.*, 2016). The magnetic properties of iron oxide NPs are influenced by factors such as size, shape, composition, crystallographic structure magnetic anisotropic energy, vacancies and defects. Among different types of nanomaterials, iron oxide nanoparticles exhibit excellent catalytic and reductive properties making them suitable for waste-water treatment. They also have the advantage of easy separation compared to other nanomaterials that require expensive centrifugation.

Iron oxide nanoparticles find applications in various fields including food science, sensors, catalysts, heavy metal and dye adsorption, data storage, electronic devices, environmental engineering, drug delivery, biomedical research, antibiotics and magnetic recording devices (Vasantharaj *et al.*, 2019). These nanoparticles have also demonstrated effectiveness against pathogenic bacteria and fungi due to their ability to generate highly reactive oxygen species (ROS) Metal oxide nanoparticles including iron oxide NPs are generally considered safe for humans and the environment. Iron oxide nanoparticles with their magnetic properties are particularly notable and can be employed in waste-water treatment, heavy metal adsorption and catalysis (Muthukumar *et al.*, 2018).

1.7.2 Green Synthesis of IONPs Using *C. maxima* Peel Extract

New methods utilizing biological sources such as microorganisms, microbial extracts/products and plant extracts have been introduced as alternatives to conventional physical and chemical methods for nanostructured carrier (NC) synthesis. The chemicals used in traditional methods often leave behind reactive and toxic residues causing environmental pollution. Researchers are actively working on developing facile, effective, sustainable, and reliable green chemistry processes for nanomaterial production. In the context of iron oxide nanoparticles, *C. maxima* peel extract was used for green synthesis. Calcium, magnesium, zinc, iron, manganese, and vitamins A, B, C, E, and K are abundant in the peel of *C. maxima*.

Biosynthesis of nanoparticles (NPs) is considered an environmentally friendly approach since it does not involve toxic agents. Studies have shown that NPs synthesized using plant products or extracts are more stable and have a faster synthesis rate compared to conventional techniques. Green approaches are eco-friendly, cost-effective, simple and do not involve toxic agents. Green synthesis of nanomaterials has gained importance due to its low cost, simplicity, availability, eco-friendliness, non-toxicity and scalability. It does not require multiple steps, high energy, high temperature, pressure, concentration or the use of toxic chemicals and it does not produce hazardous by-products. In this context, various bio-resources such as plants, bacteria, fungi, algae, yeast and viruses have been evaluated as alternative, clean and eco-friendly precursors for the preparation of small-sized and table nanoparticles (Ahammed *et al.*, 2020). The use of biomaterials as replacements for hazardous substances is a notable approach in green nanotechnology.

Utilizing different plant parts for the synthesis of metal nanoparticles is a simple and cost-effective approach.

Several studies have been conducted on the green synthesis of metal-based nanoparticles using various plant parts such as fruit extracts of *C. maxima*, *Ceynometra ramiflora*, rind of *Persea americana*, seed extracts of *Punica granatum*, flower extract of *Avicennia maria*, peel extracts of *C. maxima, C. sinensis, C. limon,* leaf extract of *C. maxima, Psidium guajava, Carica papaya* as well as cell cultures of fungi, algae and bacterial strains. Green synthesis of nanoparticles utilizes plant extracts as both reducing and capping agents eliminating the need for harmful reducing agents such as sodium borohydride, hydrogen peroxide, hydrazine and dimethylhydrazine which can have damaging effects in various applications. Plant extracts contain various phytochemicals or secondary metabolites including polyphenols, flavonoids, terpenoids, tannins, amides, aldehydes, ketones, phenolic acids, hydroxyl groups, carboxylic groups, citric acid, reducing sugars, reductases, dehydrogenase and extracellular electron shuttlers present in microbial enzymes. These compounds act as reducing and capping agents, facilitating the reduction of metal precursors and the formation of stabilized metal nanoparticles (Wei *et al.*, 2016; Rajeshkumar et. al., 2017). In this approach of green synthesis, the precursor is $FeCl_3.6H_2O$. The step involved in the bio-synthetic approach of IONPs is mentioned accordingly.

Ionization of $FeCl_3.6\ H_2O$:

$FeCl_3.6\ H_2O\ (aq) \rightarrow Fe^{3+}\ (aq) + OH^-\ (aq) + H^+\ (aq) + Cl^-\ (aq)$

In the above redox reaction, the electron donor is a plant molecule and the Fe^{3+} ion acts as electron acceptor species. Metabolites in the plant extracts act as capping and stabilizing agents between donor and acceptor species. The actual mechanism explicates the Fe^{3+} ions are trapped on the biomolecule surface (such as protein) through electrostatic interaction between the Fe^{3+} ion and the protein. In this process, Fe^{3+} ions are reduced with the help of proteins, and the secondary structure of the protein is transformed then iron nuclei formation takes place. After all, through the successive accretion of iron nuclei by the reduction of Fe^{3+} ion, the IONPs are synthesized. Even so, there is some possibility to agglomerate the IONPs because of Vander Waal's force. So, the

stabilization of IONPs is important with the counter repulsive force which is mediated through either steric or electrostatic stabilization. The secondary metabolites of the plant extract are responsible for its capping agents, giving a coated layer on the nanoparticle to resist them from agglomeration which in turn stabilizes the silver nanoparticles. Thus, the strong tendency of aggregation is countered by a strongly bounded capping agent (Khandel *et al.*, 2018).

Pomelo (*Citrus maxima*) is a popular fruit belonging to the family Rutaceae, which is grown widely in tropical and subtropical climates in Southeast Asian countries like India, China, Vietnam, Bangladesh, Malaysia, Nepal, Philippines. The pomelo tree is a perennial shrub with a longer growth cycle. Its height ranges from 5 to 15 meters. The pulp of the pomelo is yellow or pale green, while the peel is greenish-yellow, consists of a range of colors. Our immune systems are boosted by pomelo, which also prevents gaining weight and regulating blood sugar levels in diabetic people as an anti-aging medication. Every portion of the pomelo offers different advantages, such as the ability to treat swellings using a hot leaf decoction. Fruit juice can be used as a febrifuge, a type of medication that works to lower fever. Pomelo seeds are useful in treating coughs and dyspepsia additionally, fruits of Pomelo is a useful cardiotonic fruit. Also, fruit is effective at preventing Congestion issue and enhance peristalsis and digestion (Zou *et al.*, 2016).

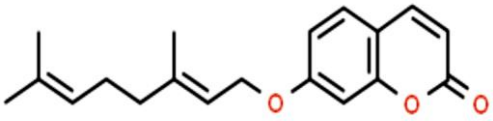

Auraptene

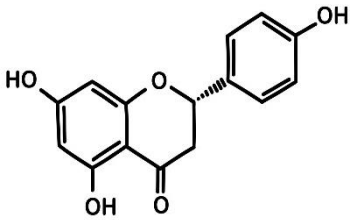

Naringenin

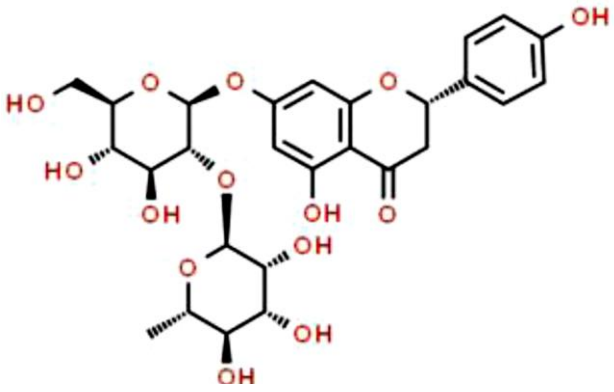

Naringin

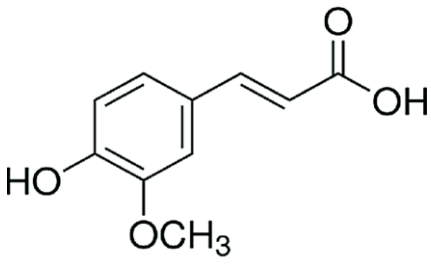

Ferulic acid

Figure 1.3: Some phytochemicals present in *Citrus maxima* peel (Zou *et al.*, 2016).

According to reports, *Citrus maxima* peel extract contains significant amounts of phenolic acids, coumarin flavonoids, rutin, and terpenoids (Figure 1.3). These substances are regarded as organic antioxidants. Furthermore, they can likewise function well as a reducing agent to create IONPs. Thus, IONPs were produced from this method are more biocompatible and appropriate for industrial and biomedical uses. Many individuals still favor using herbal remedies made from plants to heal a variety of ailments, illnesses (such as tumors and infectious diseases). Plant components (such as leaves, fruits, seeds, and bark) include various antibacterial components, such as antioxidants, phenolic substances, alkaloids, flavonoids, steroids, terpenoids, etc which is utilized for treatment (Yu *et al.*, 2016). Fresh pomelo fruit is eaten, whereas its peel is thrown away as biological waste But pomelo peel, which can make up to 30% of the fruit's weight, is regarded as a good source of important phytochemicals like pectin, cellulose, pectinoids, and essential oils. Pomelo peel extract contains flavonoids that can convert Fe^{3+} ions into metallic Fe(0) nanoparticles and additional use of other phytochemicals is possible to create films that are antibacterial and antioxidant used in medicine or food packaging.

1.8 Characterization of IONPs

Characterization of iron oxide nanoparticles is an important step to identify and determine their properties, including shape, size, structure, morphology, surface chemistry, surface area, surface charge and dispersity (Rajeshkumar *et al.*, 2017). Various advanced techniques have been developed to facilitate the characterization of IONPs in scientific research. These techniques include UV-visible spectroscopy, X-ray diffraction spectroscopy (XRD), scanning electron microscopy (SEM), zeta potential measurement, dynamic light scattering (DLS), atomic force microscopy (AFM) and transmission electron microscopy (TEM).

1.8.1 UV-Visible Spectroscopy

UV-visible spectroscopy is a convenient and rapid technique for characterizing IONPs, providing preliminary information about their properties. It is a reliable method that allows for monitoring the stability and synthesis of IONPs. Additionally, UV-visible spectroscopy is sensitive and selective making it suitable for different types of nanoparticles (Jeong, 2017). In IONPs, the valence band and conduction band are closely positioned, enabling electrons to move freely without disturbance.

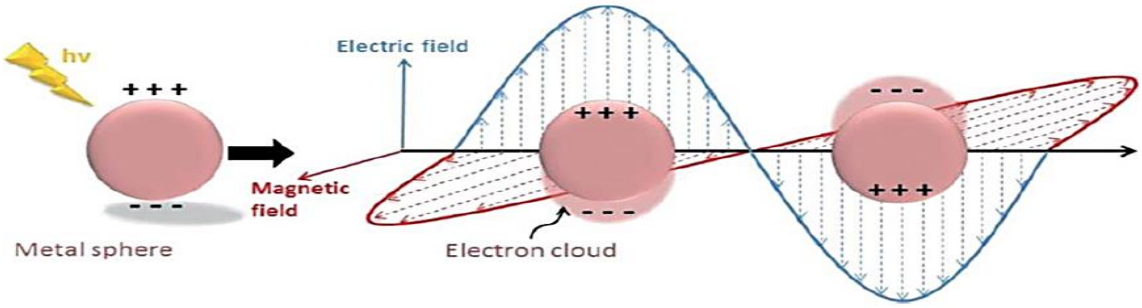

Figure 1.4: Schematic illustration of a localized surface plasmon (Peiris *et al.*, 2015).

This phenomenon generates a local surface plasmon resonance (LSPR) band as shown in figure 1.4, which results from the collective oscillation of electrons in resonance with incident light (Kumar *et al.*, 2020). Numerous studies have shown that the absorbance band of IONPs falls within the range of 200-800 nm in the UV-visible spectrum, allowing for the determination of nanoparticle sizes ranging from 4 nm to 100 nm.

1.8.2 X-Ray Diffraction (XRD)Analysis

XRD, similar to UV-visible spectroscopy is a characterization method utilized to assess various properties of nanoparticles, including the identification of chemical species, crystal or polycrystalline structure, resolution of chemicals, degree of crystallinity and particle size. When crystal nanoparticles are exposed to incident light, they disperse the light beam generating a diffraction pattern. This pattern acts as a unique identifier for the physical and chemical characteristics of the crystal. Through analysis of XRD data, the crystalline properties of IONPs, such as shape, size and structure can be determined. The mean size of the synthesized nanoparticles can be calculated using the Debye-Scherrer equation (Lin *et al.*, 2014; Kumar *et al.*, 2020).

1.8.3 Fourier Transform Infrared Spectroscopy (FTIR)

FTIR is a cost-effective and valuable spectroscopic technique employed to investigate the involvement of biomolecules present in plant extracts in the reduction of Fe^{3+} ions to IONPs. this non-invasive and straightforward analytical method is used to examine the surface chemistry of nanoparticles and ascertain whether biomolecules participate in the synthesis process. In FTIR, infrared radiation is directed at the sample which selectively absorbs and transmits specific wavelengths. The transmission and absorption of radiation generate a molecular signature that reveals the distinctive properties of the sample (Bharani *et al.*, 2013; Adhikari *et al.*, 2022).

1.9 Photocatalytic Activity of Iron Oxide Nanoparticles

Improper disposal and direct discharge of dyes and pharmaceutical pollutants from textile industries and hospital effluents have resulted in water pollution within the ecosystem (Bharani *et al.*, 2013). These toxins enter water bodies and adversely affect the global ecosystem making drinking water unsafe for consumption. Water being essential for life is crucial for both animals and human health and exposure to these toxins poses a significant risk. Currently, there are approximately 100,000 different types of dyes produced annually with a production rate of 7×10^5 tons. Textile industries alone consume around 36,000 tons of dyes per year, and up to 20% of the total dye production worldwide is lost during the dyeing process and released in textile effluents (Adhikari *et al.*, 2022). Organic dyes are known to cause damage to the central nervous system and gastrointestinal and respiratory diseases Furthermore, the increased use of antibiotics can have long-term and irreversible effects on microbes leading to genetic exchange and the accelerated development of antibiotic resistance in bacterial pathogens (Anchan *et al.*, 2019).Various methods including floatation, ion exchange, chlorination, adsorption, electrochemical degradation and photocatalytic degradation have been employed for the removal of dyes, bacteria and pharmaceutical drugs from water targeting specific pollutants like methyl orange (MO), malachite green (MG), methylene blue (MB), *E. coli*, amoxicillin, diclofenac, *S. aureus*, ciprofloxacin, sulfamethoxazole (SMX) and sulfisoxazile (SSX). However, many of these methods are costly, require equipment and do not allow for product reuse (Ardakani *et al.*, 2021; Bhuiyan *et al.*, 2020).

Among these methods, photocatalysis is favored by researchers due to its ability to degrade complex pollutants, ease of use and reproducibility. Metal oxides like zinc oxide

(ZnO), iron oxide (Fe_2O_3), titanium dioxide (TiO_2) and nickel oxide (NiO) have been extensively used as photocatalysts for pollutant degradation in wastewater. Among them, TiO_2 and ZnO are commonly used semiconductors due to their photo-electric properties. Recent studies have also shown that iron oxide nanoparticles have gained attention as an effective option for water treatment due to their low band-gap and magnetic properties, which facilitate easy recovery during the treatment process (Bibi *et al.*, 2019). These nanoparticles can be categorized into three groups based on their stability and surface area. Biologically synthesized iron oxide nanoparticles have been successfully utilized in pollutant degradation. The growing global population has led to an expansion of industries such as textiles and pharmaceuticals which require large quantities of dyes for coloration and antibiotics for medical treatment. As a result, there is an increased demand and production of these substances. Iron oxide nanoparticles have demonstrated high efficiency in dye degradation. The quality of surface water has been deteriorating due to the release of industrial effluents including dyes in recent years. More than 10,000 dyes are currently used in various industries with a significant portion employed for textile dyeing purposes (Lateef *et al.*, 2020).

Harmful substances released into the environment as effluents are causing direct or indirect damage to our surroundings. Many dyes are entering our ecosystem through water, affecting animals causing skin irritation, respiratory diseases and even cancer (Immich *et al.*, 2009). Toxicities associated with dyes such as remazol, methylene blue, methyl orange and other organic dyes include teratogenic effects on frog embryos, toxicity of enzymatic degradation metabolites, genotoxicity and phytotoxicity. Purifying textile waste effluents especially dye removal is essential for the well-being of humans and the environment. Different methods like biological processes filtration, adsorption, sedimentation, ion exchange, UV treatment and ozonation are available for purifying textile dyes. However, these methods are often costly, inaccessible or ineffective in certain cases (Hassan *et al.*, 2018). Currently, scientists are increasingly interested in photodegradation as a viable solution due to its high efficiency compared to traditional methods. To fully exploit the advantages of photodegradation, a photocatalyst with high surface area, stability, photocatalytic activity and biocompatibility is necessary. Nanomaterials based photocatalysts possess these properties and are being considered for the efficient degradation of textile dyes (Ahammed *et al.*, 2020; Hamalo-glu *et al.*, 2017).

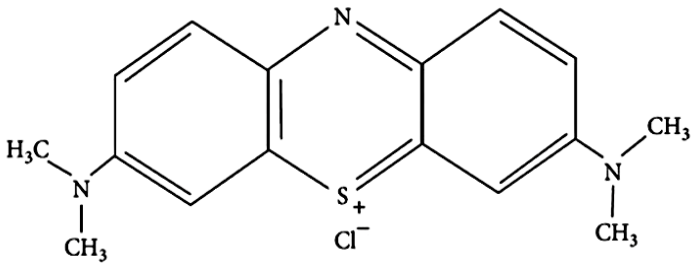

Scheme 1.1: Methylene blue

Several greener synthesis routes of iron oxide nanoparticles (IONPs) have been reported resulting in small-sized particles with a high surface area-to-volume ratio and abundant free energy on the surface. These nanoparticles interact with cells to enhance stability and overcome the band gap barrier generating electron-hole pairs. The free electrons produce reactive oxygen species in the biological system while the iron oxide nanoparticles get oxidized in the presence of air. Biological synthesis studies have demonstrated the effectiveness of iron oxide nanoparticles in degrading pollutants particularly by absorbing visible light and efficiently degrading dyes. TiO_2, a commonly used photocatalyst has a wide band gap of 3.2 eV, primarily absorbing UV light at 380 nm (only 5% of the solar spectrum). On the other hand, Fe_2O_3, an intriguing n-type semiconducting material with a band gap of 2.29 eV, exhibits good photodegradation capabilities under visible light conditions making IONPs effective as compare to TiO_2 (Hamalo-glu *et al.*, 2017).

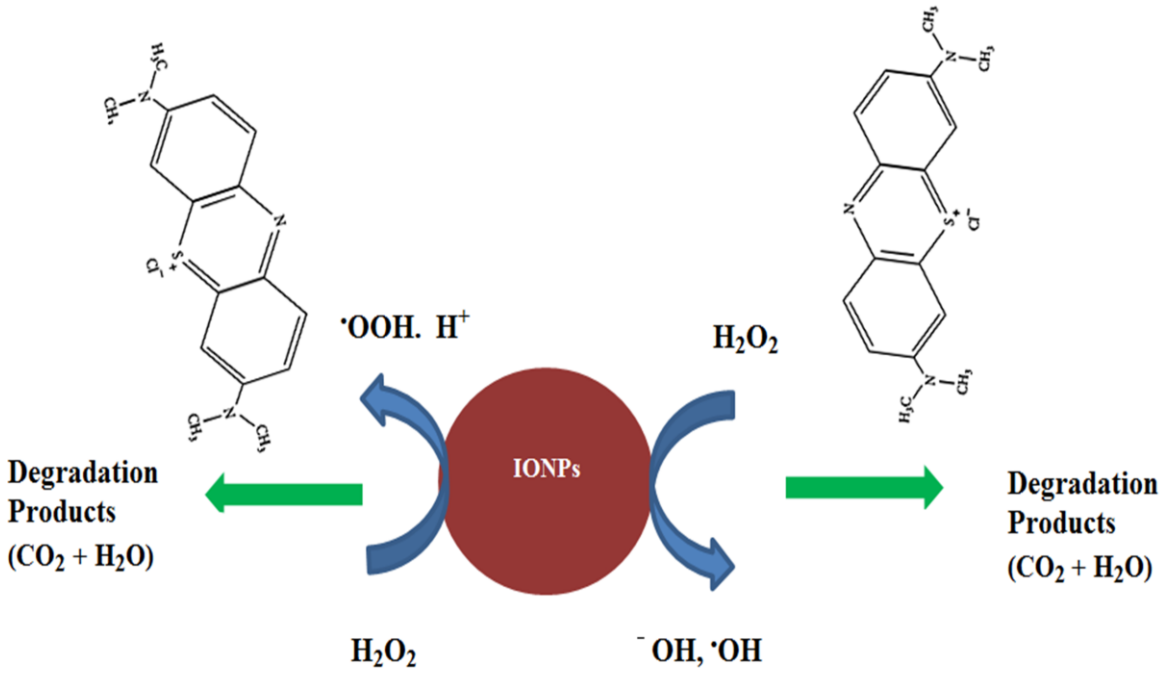

Figure 1.5: Mechanism of Photo-Fenton's process by IONPs in degradation of MB dye.

The superior photocatalytic performance of IONPs in comparison to TiO_2 can be attributed to the significant generation of electron-hole pairs caused by narrow band-gap irradiation. Due to their narrow band gap, chemical stability, high surface area and light absorption up to 600 nm, Fe_2O_3 nanoparticles can effectively excite electrons from the valence band to the conduction band and act as photocatalysts in Fenton process under visible light (Figure 1.5) serving as a precursor of Fe^{+3} ions (Akhavan *et al.*, 2009). The band gap of Fe_2O_3 nanoparticles is 2.29 eV, making them suitable for use as Fenton-like oxidants in the degradation of dyes such as methylene blue and methyl orange. Nanoparticles have shown effective photocatalytic degradation of dyes making them useful for bio-remediation purposes. Additionally, the presence of hydroxyl radicals in the Fenton system contributes to the degradation of organic dyes as the hydroxyl radicals generated by ferrite ions attack and break down the dyes (Shahwan *et al.*, 2011). In this study, we present the green synthesis of IONPs using *C. maxima* peel extract and investigate their potential for dye degradation and antimicrobial activities.

The green-synthesized IONPs demonstrated dye degradation potential against methylene blue and also exhibited good antibacterial activity against *B. subtilis*, *E. coli*, as well as antifungal activity against *Candida albicans*. Nanotechnology is a rapidly advancing field that addresses gaps in modern technologies. Advanced oxidation processes such as Photo-Fenton oxidation are promising techniques for decolorizing and mineralizing various dyes transforming them into biodegradable or harmless substances (Shahwan *et al.*, 2011). Photo-Fenton oxidation is a catalytic process that uses a mixture of hydrogen peroxide and ferrous ions (Equation i) and the addition of UV or artificial light (Equation iv) enhances dye de-colorization by facilitating the formation of hydroxyl radical (•OH). The primary reaction in the photo-Fenton process involves the Fenton reaction, photolysis of hydrogen peroxide, and photo-reduction of ferric ions as represented by the following reactions (Wanakai *et al.*, 2019):

$$Fe^{2+} + H_2O_2 \rightarrow \bullet OH + Fe^{3+} + OH^- \quad \text{(i)}$$

$$Fe^{3+} + H_2O_2 \rightarrow Fe^{2+} + OOH^{\cdot} + H^+ \quad \text{(ii)}$$

$$Fe^{2+} + OH^{\cdot} \rightarrow Fe^{3+} + OH^- \quad \text{(iii)}$$

$$H_2O_2 + hv \rightarrow OH\bullet + OH^{\cdot} \quad \text{(iv)}$$

$$Fe^{3+} + H_2O + hv \rightarrow Fe^{2+} + {}^{\bullet}OH + H^+ \quad \text{(v)}$$

1.10 Anti-microbial Activity of Iron Oxide Nanoparticles

The antimicrobial activity of IONPs against both gram-negative and gram-positive bacteria and fungi has been demonstrated in several studies. IONPs exhibit no toxicity towards eukaryotic cells suggesting their potential as next-generation antimicrobial agents with high biocompatibility. Iron plays various biological roles but can also catalyze the Fenton reaction and generate reactive oxygen species (ROS) that can damage DNA, lipids and proteins (Groiss *et al.*, 2017). Similarly, IONPs exert their antimicrobial activity by damaging bacterial cells through the same mechanisms. The small size of nanoparticles enables them to inhibit DNA replication by inactivation topoisomerase. IONPs possess magnetic and paramagnetic properties with super-paramagnetic IONPs exhibiting high paramagnetic activity. In the presence of alternating magnetic fields, they induce cell death and destroy biofilms through mechanisms such as vibration damage, local hyperthermia and ROS generation.

The factors mentioned above lead to the dissociation of bacteria from biofilms, damage to the bacterial cell wall, membrane rupture and ultimately bacterial death (Al-Matar *et al.*, 2018). IONPs have demonstrated efficacy against both gram-positive and gram-negative bacteria, making them useful as antibacterial agents in various applications including biomedical applications, contrast agents for MRI scans and wastewater treatment. The mechanism underlying their antibacterial effect is still a subject of debate but several hypotheses have been proposed. The positive charge of ferric ions is believed to play a crucial role in their antibacterial activity. Additionally, due to their small size compared to large biological molecules such as enzymes, receptors and antibodies, metal nanoparticles can interact effectively with bacterial cell membranes and other biological entities, thanks to their unique physical and chemical properties. The antimicrobial activity of nanoparticles is not fully understood but various mechanisms have been suggested. Nanoparticles have been reported to induce oxidative stress in gram-positive bacteria cells by generating excessive reactive oxygen species and releasing antimicrobial metal ions from their surface. Moreover, the abrasive nature of nanoparticles can damage bacterial membranes, contributing to their antimicrobial properties (Groiss *et al.*, 2017).

In this study, iron oxide nanoparticles were synthesized by reducing a 0.1M ferric chloride solution with *C. maxima* aqueous peel extract in a 1:1 ratio which served as a reducing agent. The synthesized nanoparticles were characterized using Fourier

Transform Infrared Spectroscopy (FTIR), UV-visible spectroscopy and XRD analysis. The synthesized IONPs exhibited significant antimicrobial activity against gram-negative (*E. coli*) and gram-positive (*B. subtilis*) bacterial strains as well as fungal strains (*C. albicans*). Additionally, the IONPs demonstrated excellent photocatalytic activity in the Photo-Fenton process utilizing H_2O_2 (30%) for the degradation of Methylene Blue dye.

1.11 Toxicity of Iron Oxide Nanoparticles

Regarding the toxicity of iron oxide nanoparticles, although they are widely utilized in various applications such as biomedical, agriculture, catalysis, drug delivery, sensors, electronics, environmental protection, water purification and pigments & coatings their release into the environment through dermal contact, ingestion and inhalation raises concerns. Ultra small IONPs (92.3 and 4.2 nm) can induce significant toxicity by specifically triggering acute oxidative stress in multiple organs. However, IONPs with sizes larger than 9.3 nm have shown no obvious toxicity with a lethal dosage of 100 mg/kg in mice through intravenous injection (Laffon *et al.*, 2018).

In recent years, FDA-approved nano-medicines particularly magnetic IONPs have found extensive use in biomedical applications such as drug delivery, MRI contrast agents, thermal ablation therapy and in vivo cell tracking. These applications require biocompatible materials. However, the toxicity of IONPs is still not thoroughly explored and for in vivo applications, magnetic nanoparticles should exhibit non-toxicity and compatibility with the human body (Maxim *et al.*, 2018). Nanoparticles used in fluids tend to degrade in the body highlighting the importance of understanding their overall toxicity and the interactions of both intact nanoparticles and their degraded products within the body. Certain nanoparticles have shown toxic effects such as inflammation, ulceration, cytotoxicity (reduced growth rate and viability) and neurobehavioral alterations in plant and animal cell line models. The toxicity of nanoparticles is attributed to their specific characteristics, including a high surface-to-volume ratio, chemical composition, size and dosage, retention in the body, immunogenicity, organ-specific toxicity and breakdown and elimination processes (Gang *et al.*, 2012). Due to limited comprehensive data and significant study parameters, the in vivo toxicity of plant-based synthesized nanoparticles is not yet clearly understood. Further research should be conducted to explore if plant-based phytochemicals involved in capping and stabilizing nanoparticles can effectively reduce their toxicity.

1.12 Statement of Problem

Iron oxide nanoparticles have been used in a variety of fields, such as food science, sensors, catalysts, heavy metals and dye adsorption, data storage, electronic devices and biomedical research. Iron oxide nanoparticles are a type of metal oxide that is usually regarded as harmless for both humans and environment. However, according to the literature survey, very less research has been carried out on green synthesis of IONPs from *C. maxima* peel extracts. So, to overcome this problem, the present work has been carried out by green synthesis which is cost-effective, eco-friendly and biocompatible.

1.13 Hypothesis

It is hypothesized that iron oxide nanoparticles (IONPs) can be synthesized using *C. maxima* peel extract and these synthesized nanoparticles can be utilized for the photocatalytic degradation of organic dyes and it can also be employed for anti-microbial applications.

1.14 Research Objectives

1.14.1 General Objective

To synthesize iron oxide nanoparticles using *C. maxima* peel extract and explore their applications in the photocatalytic degradation of organic dyes and anti-microbial activities.

1.14.2 Specific Objectives

1. To prepare *C. maxima* peel extract.
2. To synthesize iron oxide nanoparticles using *C. maxima* peel extract.
3. To characterize the IONPs through UV-visible spectroscopy, FTIR and XRD analysis.
4. To determine the average size of the synthesized iron oxide nanoparticles.
5. To investigate the photocatalytic degradation of organic dyes and evaluate the antimicrobial activity of the IONPs.

CHAPTER 2

2. LITERATURE REVIEW

Various methods have been developed to synthesize metal nanoparticles, including reduction reactions, photochemical reactions, thermal decomposition, electrochemical methods, sol-chemical methods, and microwave-assisted methods. Although these techniques are effective and yield high-quality nanoparticles, they often require toxic chemicals that contribute to environmental degradation. Additionally, these synthetic procedures can be costly and handling of hazardous chemicals can be challenging. As a result, there is a growing interest in developing easy, inexpensive, safe, eco-friendly, and biocompatible methods for synthesizing metallic nanoparticles using biological species such as plant parts (leaves, stems, fruits, fruit peels). fungi, actinomycetes, and enzymes. These green synthesis methods aim to replace the existing costly commercial synthetic or chemical methods of manufacturing nanoparticles. Several research articles have been published on the green synthesis of iron oxide nanoparticles (INOPs) and their applications in the photocatalytic degradation of organic dyes and antimicrobial activity.

Bibi *et al.,* (2019) studied the green synthesis of iron oxide nanoparticles using pomegranate seeds. The nanoparticles were characterized using UV-vis, XRD, EDX, SEM, and AFM techniques, and their particle size ranged from 25 to 55 nm. The synthesized Fe_2O_3 nanoparticles exhibited excellent photocatalytic activity against reactive blue under UV light irradiation, achieving a maximum degradation rate of 95.08% within 56 minutes of reaction time (Bibi *et al.*, 2019).

Vasantharaj *et al.*, (2019) reported the biosynthesis of iron oxide nanoparticles using leaf extract of *Ruellia tuberosa*. The nanoparticles were characterized using UV-visible spectroscopy, FTIR spectroscopy, FESEM-EDX, TEM, DLS, and DSC techniques. The calculated average size of FeONPs against gram-negative bacteria (*E. coli*, *Klebsiella pneumoniae)* and lesser antibacterial activity against gram-positive bacteria (Staphylococcus aureus). The FeONPs synthesized demonstrated a strong photocatalytic ability, achieving up to 80% degradation of crystal violet dye under solar irradiation (Vasantharaj *et al.*, 2019).

Wanakai *et al.*, (2019) studied the Catalytic degradation of methylene blue by iron nanoparticles synthesized using *Galinsoga parviflora*, *Conyza bonariensis and Bidens pilosa* leaf extracts which was characterized by using UV–vis spectrophotometer, FT-IR

spectrophotometer, X-ray Fluorescence (EDXRF), X-ray diffractometer (XRD), and scanning electron microscope (SEM). The UV–vis spectrum of $FeCl_3$ had a adsorption peak at 320 nm and the leaf extracts at 267 nm, 288 nm and 286 nm for *Galinsoga parviflora, Bidens pilosa* and *Conyza bonariensis* respectively which disappeared upon addition of *G. parviflora, C. bonariensis* and *B. pilosa* extracts confirming formation of iron nanoparticles. XRD data revealed presence of a large amorphous coating that masked iron peaks which have been reported to be of iron oxides. The *Conyza bonariensis* (CbNPs), *Bidens pilosa* nanoparticles (BpNPs) and *Galinsoga parviflora* nanoparticles (GpNPs) synthesized were good biocatalysts as they degraded the Methylene blue dye by 86%, 84.3% and 92% respectively (Wanakai *et al.*, 2019).

Bhuiyan *et al.*, (2020) reported the green synthesis of iron oxide nanoparticles using *Carica papaya* leaf extract. The nanoparticles were characterized using techniques such as FTIR, XRD, FESEM, EDX, and TGA. The average diameter of the nanoparticles was determined to be 21.59 nm, and the average crystallite size was found to be 4.58 nm. The synthesized α-Fe_2O_3 nanoparticles demonstrated efficient degradation of remazol yellow RR dye under sunlight, with 77% of the dye degraded within 6 hours at a dosage of 0.8 mg/L. The nanoparticles also exhibited moderate antibacterial activity against specific gram-negative and gram-positive bacterial strains, showing toxicity at high doses but excellent activity against BHK-21 and HELA cell lines (Bhuiyan *et al.*, 2020).

Jamzad *et al.*, (2020) investigated the green synthesis of iron oxide nanoparticles using the aqueous extract *Laurus nobilis* L. leaves. The synthesis was confirmed through UV-visible spectroscopy, FT-IR spectroscopy, XRD analysis, SEM, TEM, and EDS spectroscopy. The nanoparticles were found to be crystalline, mostly spherical, and partly hexagonal, with an average size of 8.03 ±8.99 nm from TEM analysis. The crystalline size of the synthesized nanoparticles was estimated to be approximately 21.5 nm using Scherers equation from XRD analysis. The nanoparticles showed excellent results against the gram-negative bacteria *E. coli*, gram-positive bacteria *S. aureus,* and moderate activity against the gram-positive bacterium Listeria monocytogenes. They also exhibited high inhibition zones against two fungi, *Aspergillus flavus* and *Penicillium spinulosum* (Jamzad *et al.*, 2020).

Jose *et al.*, (2020) studied the photocatalytic degradation of methylene blue using iron oxide nanoparticles synthesized using *Annona muricata* leaf extract. The nanoparticles were characterized using UV-visible spectroscopy, TEM, SEM, X-ray diffraction (XRD),

and FTIR spectroscopy. The characterization revealed that the nanoparticles exhibited aggregated, irregular rough surfaces, and spherical shapes, with an average size of 20 nm. the synthesized iron oxide nanoparticles showed good antibacterial activity against the tested pathogens and also demonstrated significant photocatalytic activity in the degradation of methylene blue (Jose *et al.*, 2020).

Kirdat *et al.*, (2020) reported the synthesis and characterization of ginger (*Z. officinale*) extract-mediated iron oxide nanoparticles. The nanoparticles were characterized using UV-visible spectroscopy, FTIR spectroscopy, XRD technique, and SEM analysis. The average size of the nanoparticles was determined to be 5.10 nm from XRD analysis. The synthesized nanoparticles from ginger extract demonstrated good antibacterial activity against the gram-negative bacteria *E. coli*, with inhibition zones measuring 20 mm and 22 mm in diameters at concentrations of 80 µl and 100 µl, respectively (Kirdat *et al.*, 2020).

Kumar et. al., (2020) reported the characterization and application of biosynthesized iron oxide nanoparticles using *Citrus paradisi* peel extract which was characterized by using UV–visible spectroscopy, Dynamic Light Scattering (DLS), Transmission electron microscopy (TEM) with selected area electron diffraction (SAED), X- ray diffraction (XRD) and Thermogravimetric analysis (TGA).The average size of iron oxide nanoparticles was 27.1 ± 13.9 nm from the DLS study and 28–32 nm from TEM analysis respectively that confirms the spherical shape, aggregating nature of iron oxide nanoparticles. Likewise, XRD analysis confirmed the mixture of Fe_3O_4, α-Fe_2O_3 and γ-Fe_2O_3 nanoparticles in existence. The TG analysis showed that the nanoparticles contain 76% metal,16% adsorbed moisture and 8% capping ligand. The synthesized iron oxide nanoparticles exhibited antioxidant activities against 1, 1-diphenyl-2-picrylhydrazyl (DPPH) (> 15%, 100 µg) and also they were used for the degradation of different synthetic dyes such as Methyl Rose, Methylene Blue and Methyl Orange from which the different degradation percentages were obtained as for the dyes MR (96.65%, 50 mg/L), MB (80.76%, 10 mg/L) and MO (89.64%,10 mg/L), respectively for 6 hr at 25 °C (Kumar et. al., 2020).

Qasim *et al.*, (2020) carried out a green synthesis of iron oxide nanorods from *Withania coagulans* extract, which combined biological and chemical techniques to improve photocatalytic degradation and antibacterial activity. The characterization involved UV-visible spectroscopy, FTIR spectroscopy, XRD analysis, SEM, and TEM techniques. XRD and SEM analysis revealed that the nanorods synthesized using *Withania* extract

exhibited a highly crystalline nature with an average size of 16 ± 2 nm, while those synthesized using the chemical method displayed a less crystalline structure with an amorphous nanostructure and an average size of 18 ± 2 nm. The degradation of safranin dye in the presence of *Withania coagulans*-based nanorods showed a 30% higher efficiency compared to chemically synthesized nanorods, as evidenced by the gradual decrease in peak intensity under sun illumination at 553 nm and 550 nm, respectively. Moreover, the *Withania coagulans*-based nanorods exhibited effective antibacterial activity against *S. aureus* and *P. aeruginosa*, outperforming the nanorods synthesized nanorods were more effective and functionally efficient than those prepared using the chemical precipitation-based method (Qasim *et al.*, 2020).

Adhikari *et al.*, (2022) reported the green synthesis of iron oxide nanoparticles using *Psidium guajava* L. leaves. The nanoparticles were characterized using UV-visible spectroscopy, FTIR, XRD, XPS, EDX, FESEM, HR-TEM, and Zeta potential analysis. The average crystallite size was determined to be 21.75 nm. The synthesized IONPs demonstrated the ability to degrade dye efficiency (Adhikari *et al.*, 2022).

Mahlaule-Glory *et al.*, (2022) conducted the biosynthesis of iron oxide nanoparticles using M. burkeana extract. The nanoparticles were characterized using UV-vis, XRD, BET, SEM, EDS, and TGA. The crystallite sizes were found to be around 60 nm, and the nanoparticles exhibited a rod-like and mesoporous structure. The synthesized IONPs (Fe_3O_4) were effective in degrading organic and antibiotic pollutants, achieving a degradation rate of 99% for methylene blue and 60% for sulfisoxazole. They also demonstrated greater potency against gram-positive (*E. coli*) bacterial strains compared to gram-negative (*S. aureus)* strains (Mahlaule-Glory *et al.*, 2022).

2.1 Research Gap

Research on iron oxide nanoparticles (INOPs) has predominantly focused on their chemical synthesis and biosynthetic processes using various plants. These nanoparticles have been investigated for their potential applications in minimizing hazards and addressing issues related to industrial wastewater such as the detection of organic chemical wastes. However, there are still limited researches and comprehensive data on the biosynthetic process of synthesizing IONPs using *C. maxima* peel extract are not available. Moreover, limited applications have been explored. Some experiments have

reported the synthesis of IONPs using *C. maxima* peel extract with applications in biomedical fields, catalysis, water purification, photocatalytic degradation of organic dyes and hazardous metal detection. However, detailed reports on the multiple applications of IONPs are still in high demand. Therefore, this research project will primarily focus on the synthesis of IONPs using *C. maxima* peel extract and their subsequent use in anti-microbial applications and photocatalytic degradation of dyes with the aid of a UV-visible spectrophotometer.

CHAPTER 3

3. RESEARCH METHODOLOGY

The research was conducted entirely through laboratory experiments, and the data obtained were analyzed using various spectroscopic techniques. The research followed a systematic approach based on objectivity, generality, and verifiability, relying on the experimental results.

3.1 Research Design

In any scientific experimentation and research, reliable conclusions and valid inferences are derived from careful analysis and observations. Therefore, it is crucial to plan and design the study appropriately before conducting the experiments. The study design involves the systematic organization of data and ensures precision and reliability. During laboratory work, it is essential to adhere to standard protocols and maintain a controlled environment to minimize errors. The research design outlined below was employed for the synthesis, characterization, and application of iron oxide nanoparticles.

.

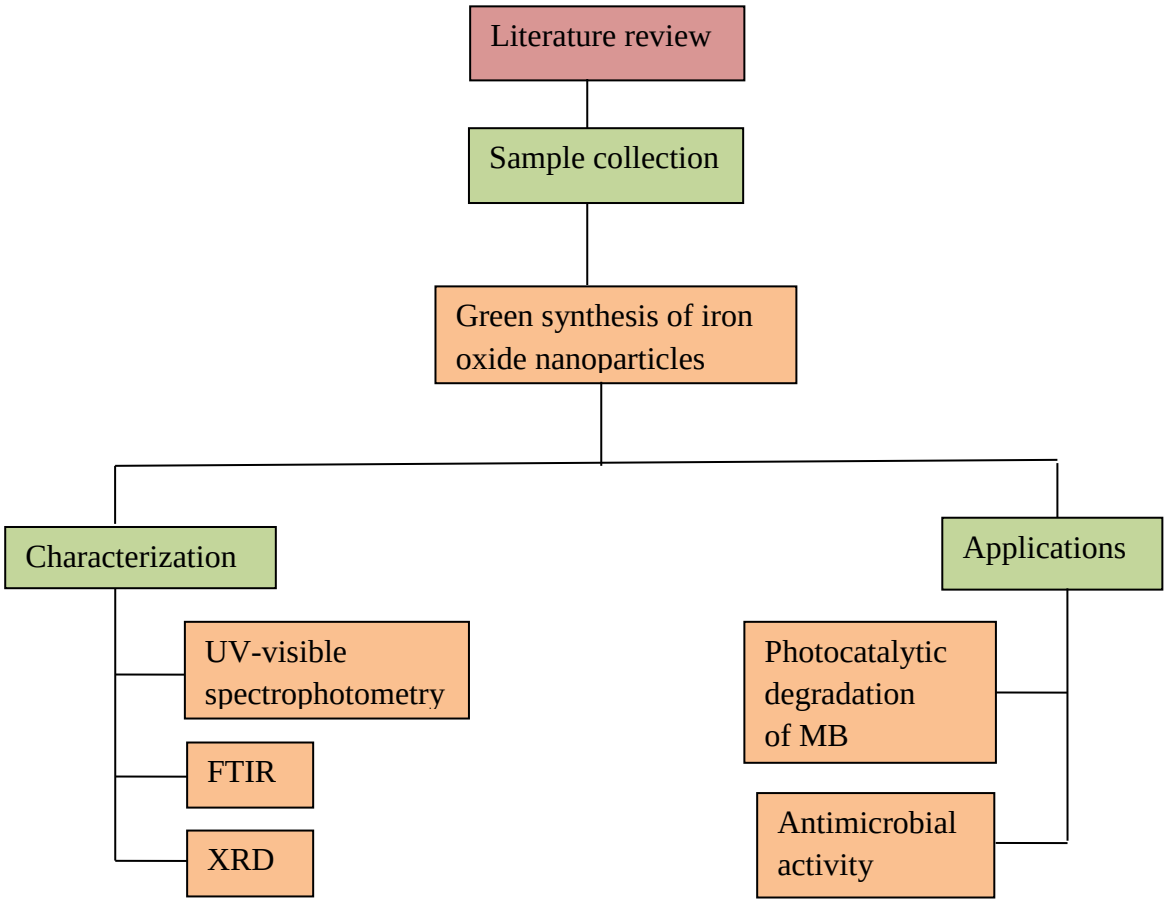

Figure 3.1: Flow chart showing the research work plan.

3.2 Plant Materials Classification

Kingdom: Plantae

Division: Magnoliophyta

Class: Magnoliopsida

Order: Sapindales

Family: Rutaceae

Genus: *Citrus*

Species: *maxima*

Figure 3.2: Photographic image of *Citrus maxima*.

3.3 Identification of the Plant

C. maxima fruit was bought from the local market in Kathmandu, Nepal. Its common name is Pomelo and it has various names like grapefruit, shaddock, *C. grandis* and *C. paradisi*. It is a citrus fruit from South East Asia. It is pale green or yellow when ripe. Its flesh is sweet and white. The rind is very thick and spongy. It is the largest citrus fruit usually 15-25 cm in diameter. It weighs 1 to 2 kg (2.2 to 4.4 lb).

3.4 Solvents and Chemicals

The chemicals and solvents used in this research work include Ferric chloride hexahydrate ($FeC1_3.6H_2O$) from Fisher Scientific, ethanol, distilled water, Whatman filter paper No.1, NaOH, and 30% H_2O_2 from Fisher Scientific. All these materials were obtained from the chemistry laboratory without further purification.

3.5 Instrumentation

The following instruments were used during this research work: UV-visible spectrophotometer (LT- 2802, Labtronics), X-ray diffraction (XRD) (Bruker, D2 Phaser Diffractometer), Hot air oven (UN30, Elite Oven), Mechanical grinder (LM-05, Chinetti), Digital weighing balance (ASN-224, Phoenix instrument), Magnetic stirrer hot plate (L34, Labinco), FTIR instrument (10.6.2, Perkin Elmer), Refrigerator, Centrifuge (SORVALL ST 8R Centrifuge), Digital pH meter (LT-11, Labtronics) and other relevant instruments.

3.6 Biosynthesis of Iron Oxide Nanoparticles

The synthesis of iron oxide nanoparticles using *C. maxima* peel was carried out with the following procedures with some modifications.

3.6.1 Plant Extract Preparation

C. maxima fruits were bought from the local market in Kathmandu. The fruits were washed with tap water and then with distilled water. Then, the peel was removed from fruit with the help of a knife and left for drying in sunlight for 7 days. The dried peels were ground to make a powder using an electrical blender and the remaining peels were stored in a polythene bag for future use. About 20 grams of the fine powder sample was heated in 600 mL of distilled water on a magnetic stirrer hot plate at 80°C for 30 minutes. The mixture was then filtered through Whatman Filter Paper No. 1 after cooling and the collected filtrate was finally referred to as *C. maxima* peel extract. The extract was used for the experiments and the remaining extract was stored at 4°C in the refrigerator for further use.

3.6.2 Preparation of Ferric Chloride Hexahydrate (Iron Chloride) Solution

To create a 0.1M concentration of iron chloride solution, 6.8 grams of $FeCl_3.6H_2O$ were dissolved in 250 mL of distilled water. The resulting solution was then stored in a dark place away from sunlight.

3.6.3 Biosynthesis of Iron Oxide Nanoparticles

In the biosynthesis process, 50 mL of *C. maxima* peel extract was slowly added drop by drop to 50 mL of $FeCl_3.6H_2O$ in a 1:1 molar ratio at a temperature of 80°C on a magnetic stirrer hot plate. The mixture was stirred for one hour on a magnetic stirrer at a constant speed of 850 rotations per minute. The formation of a black-colored solution confirmed the synthesis of iron oxide nanoparticles (IONPs) as the color change was attributed to the surface plasmon resonance (SPR) effect and the conversion of Fe^{3+} ions to Fe_2O_3 NPs by the aqueous *C. maxima* peel extract. The initial yellow color was mainly due to the *C. maxima* peel extract which gradually faded away and turned black as the concentration of IONPs increased. Subsequently. After then, 1M NaOH was added to the reaction mixture until the pH reached 11, as measured by a pH meter. The formation of nanoparticles was confirmed using a UV-visible spectrophotometer which exhibited a characteristic

maximum peak at a wavelength of 353 nm. The synthesized IONPs were then stored in the refrigerator for further uses in separation, purification and characterization.

3.6.4 Purification and Separation of Iron Oxide Nanoparticles

The synthesized IONPs were separated and purified through centrifugation at 8000 rpm for 10 minutes. The resulting pellet was washed 2-3 times with distilled water and then with ethanol to remove impurities. Finally, the nanoparticles were dried in a hot air oven at 80°C for 24 hours before being stored in a sealed container for subsequent characterization and applications. The synthetic procedure involved in this work is illustrated in the (figure 3.3).

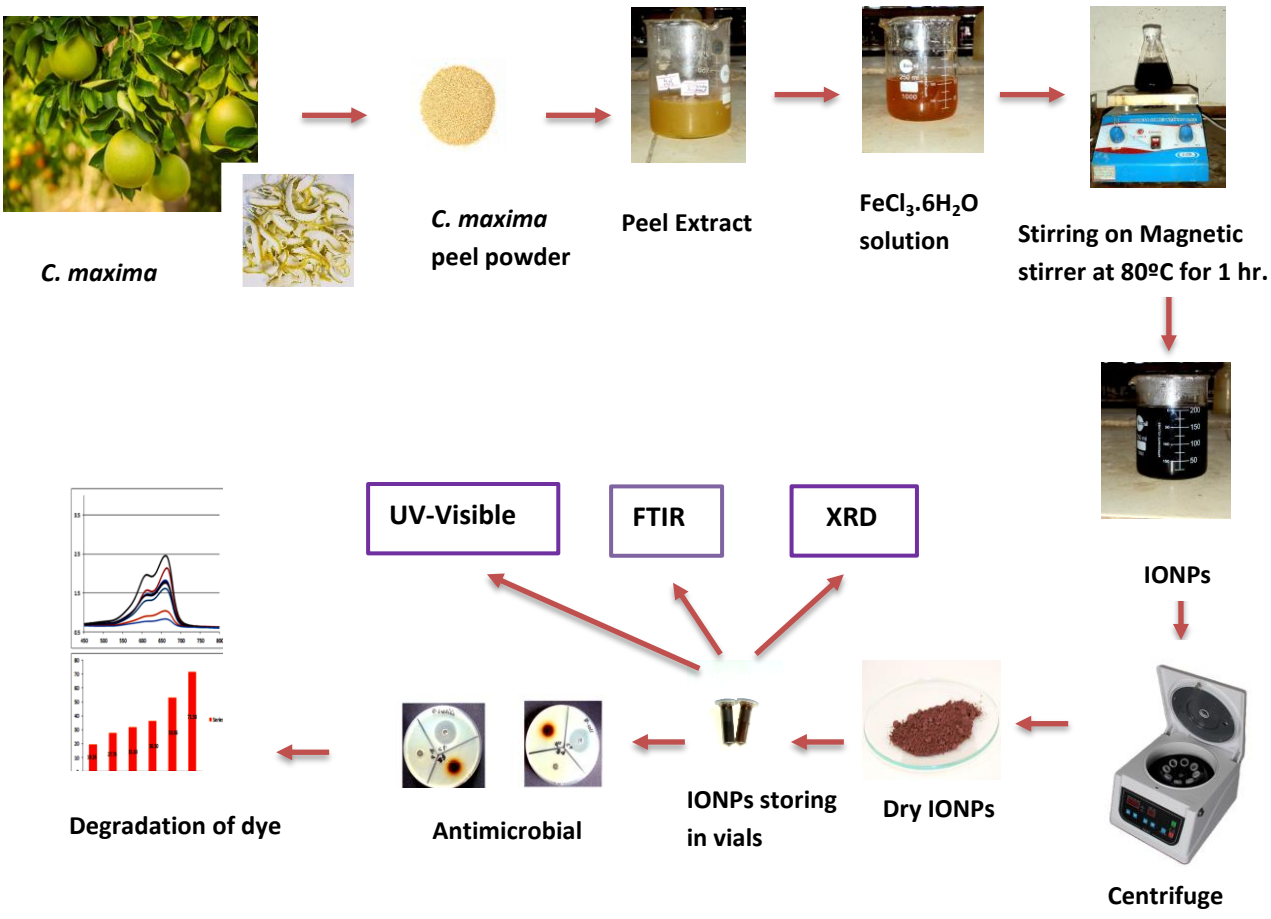

Figure 3.3: Schematic diagram showing the green synthesis of IONPs.

3.7 Photocatalytic Activity of IONPs

IONPs possess a significant capability for degradation such as methylene blue (MB), ramazol, methyl orange (MO) and various other organic dyes. This study primarily focused on the degradation of methylene blue dye using IONPs in conjunction with

hydrogen peroxide (H_2O_2) in the Photo-Fenton process. Initially, a stock solution of methylene blue was prepared by dissolving 10 mg of MB in 1L of distilled water to achieve a 10-ppm concentration. Subsequently, 100 mL of the MB solution was taken in a 250 mL beaker and varying amounts of IONPs (5 mg, 10 mg and 20 mg) were added. The mixture was kept in the dark for 30 minutes to establish equilibrium with the nanoparticles after which 0.2 mL of 30% H_2O_2 was added and stirred continuously on a magnetic stirrer for 30 minutes. The UV-visible spectrophotometer recorded the absorbance of the solution and was noted as A_0 absorbance. The solution mixture was then exposed to sunlight and the absorbance of the sample solution was monitored at specific time intervals. The color change of the solution from intense blue to light blue and eventually colorless was observed after 1.5 hour of solar irradiation and the absorbances (A_{10}-A_{90}) were recorded from 10 to 90 minutes after every time interval of 10 minutes. A photographic image of the color change of methylene blue was also captured. The progress of the reaction in the resulting solution was monitored by measuring the absorbance at different time intervals (T). The efficiency of dye degradation was calculated using the formula:

$$\text{Efficiency (\%)} = ((A_0 - A_t) / A_0) \times 100$$

Where, efficiency (%) represents the degradation efficiency of the dye; A_0 is the absorbance of the dye solution at zero time and A_t is the absorbance of the dye solution in suspension after time T.

3.8 Anti-Microbial Activity of IONPs

The anti-microbial activity of IONPs synthesized from *C. maxima* peel extract was evaluated using the Ager Well Disc Diffusion method. For the antibacterial analysis, a new culture of test organisms (*Bacillus subtilis* and *Escherichia coli*) was spread on the MHA plate using a sterile cotton swab. Separate sterile blank anti-microbial susceptibility discs were loaded with IONPs (20 µL, 25 mg/500 µL), neomycine (20 µL, 1 mg/mL) as positive control and plant extract. These discs were then placed on the MHA plate and incubated at 37°C for 18-24 hours. After incubation, the zone of inhibition (ZOI) was measured and recorded. Similarly, for antifungal analysis, a new culture of the test organism *Candida albicans* was spread on the PDA plate using a sterile cotton swab. Sterile blank anti-microbial susceptibility discs were loaded with IONPs (20 µL, 25

mg/500 µL), clotrimazole (20 µL, 1 mg/ml) as positive control) and plant extract. These discs were incubated at 37°C for 18-24 hours and the ZOI was measured and recorded.

The anti-microbial activity of synthesized IONPs was carried out at Himalaya Research Institute of Biotechnology Pvt. Ltd., Srijananagar, Bhaktapur, Nepal.

3.9 Characterization of IONPs

Characterizing IONPs is a crucial step in identifying and understanding the properties of the nanoparticles. Various analytical techniques are employed to determine the nanoparticles' size, shape, structure, morphology, surface chemistry, surface charge, surface area, and disparity. UV-visible spectroscopy and scanning electron microscopy are used for this purpose. Scanning electron microscopy (SEM), Transmission electron microscopy (TEM), Atomic Force Microscopy (AFM), Fourier Transform Infrared (FTIR) as well as X-ray diffraction (XRD) and energy dispersive X-ray (EDX) analysis are utilized for the characterization of IONPs.

3.9.1 UV-Visible Spectroscopy

UV-visible spectroscopy provides a quick and convenient method for characterizing IONPs, allowing for the determination of their optical properties. It is a sensitive and selective technique that aids in monitoring the stability and synthesis of IONPs. UV-visible spectroscopy was employed in this study to characterize the properties of IONPs using *C. maxima* peel extract at different time intervals over one week. The technique predicted maximum peaks within the range of 200 to 800 nm indicating the absorption band of IONPs. It was also utilized to monitor the degradation of methylene blue mediated by IONPs, predicting maximum peaks at different wavelengths.

3.9.3 X-Ray Diffraction (XRD)

XRD is a characterization technique that provides quantitative identification of chemical species, crystal or polycrystalline structure, resolution of chemicals, degree of crystallinity, and particle size. In XRD, crystal nanoparticles scatter incident light resulting in a diffraction pattern that reveals the physical and chemical properties of the crystal. In this research, X-ray diffraction (XRD) analysis was used to determine the crystallinity and phase diversity of the synthesized IONPs. The analysis was conducted using a Bruker, D2 Phaser Diffractometer. Xpert high-score software with a search and

match facility was employed for phase determination. The crystalline grain size of the IONPs was calculated using Scherrer equation:

$$D = k\lambda/\beta\cos\theta$$

Where,

D = Crystalline size

λ = Wavelength of x-ray radiation (0.154 nm)

k = Dimensionless shape factor with a value close to unity, (0.94)

β = Full width at half maximum, FWHM (in radians)

θ = Bragg's angle (half of the 2θ value of chosen peak (in radians)

The XRD analysis of the synthesized IONPs was carried out at the Nepal Academy of Science and Technology (NAST), Khumaltar, Lalitpur, Nepal.

3.9.4 Fourier Transform Infrared Spectroscopy (FTIR)

FTIR is an economical and valuable spectroscopic technique used to investigate the role of biomolecules present in the plant extract for the reduction of Fe^{3+} ions to Fe^{0} nanoparticles. This technique provides insight into the surface chemistry of the IONPs and is a simple analytical tool for this purpose. To determine the involvement of biomolecules in the synthesis of nanoparticles, Fourier Transform Infrared Spectroscopy (FTIR) is employed. This technique involves subjecting the sample to infrared radiation where some of the radiation is absorbed while the rest transmits through it. By analyzing the transmission and absorption of radiation, a molecular fingerprint is created providing a specific identity of the sample. In this study, IONPs and *C. maxima* peel extract were analyzed using an FTIR spectrometer (Perkin-Elmer LS-55-Luminescence spectrometer) in the range of 4700-400 cm^{-1}. This analytical technique offers insights into the composition and presence of functional groups on the surface of IONPs and in the *C. maxima* peel extract.

3.10 Phytochemical Screening

The qualitative phytochemical analysis of *C. maxima* peel extract was carried out to determine the presence of flavonoids (alkaline reagent), alkaloids (Dragendorff's), tannins (Few drops of $FeCl_3$), phenolics (lead acetate, alkaline reagent test), saponins (foam test), triterpenes (Liberman test) and carbohydrates (Molisch's test).

3.10.1 Preparation of Solvent Extract

The aqueous extract of *C. maxima* peel was prepared by dissolving 10 g of the dried peel powder in 100 mL of distilled water and heated on magnetic stirrer hot plate at 80ºC for 1 hour. After that, extract was filtered by Whatman filter paper No.1 and stored in an airtight container and kept in a refrigerator at 4ºC for further use.

3.10.2 Phytochemical Analysis

Different tests were performed by using *C. maxima* aqueous peel extract for preliminary estimation of phytochemicals present in the plant extract.

Alkaloids Tests

Mayer's Test

About 1 mL of aqueous peel extract was taken in a clean test tube and few drops of Mayer's reagent was added to it and then 0.1% HCl was added. The yellow colour confirmed the presence of alkaloids.

Wagner's Test

1 mL of aqueous peel extract was taken in a test tube and few drops of Wagner's reagent was added to it. The reddish-brown precipitates appeared that confirmed the presence of alkaloids.

Dragendroff's Test

1 ml of aqueous peel extract was taken in a test tube and few drops of Dragendroff's reagent was added to it. Appearance of reddish-brown precipitates confirmed the presence of alkaloids.

Flavonoids Tests

Method-1: 1 mL of aqueous peel extract was taken in a test tube and 1-2 mL of conc. HCl was added to it and then magnesium ribbon was added. The appearance of pink colour showed the presence of flavonoids.

Method-2: 1 mL of aqueous peel extract was taken in a test tube and 10% of $Al(OH)_3$ was added to it. The yellow fluorescence appeared that confirmed the presence of flavonoids.

Saponins Test

2 mL of aqueous peel extract was taken in a test tube and few mL of sterile distilled water was added to it and shaken vigorously for few seconds. Then, it was allowed to stand undisturbed for few minutes. The honeycomb froth like persistent over the liquid indicated the presence of saponins.

Tannins Test

1 mL of aqueous peel extract was taken in a test tube and 0.1% $FeCl_3$ solution was mixed to it. The brownish-green colour appeared which confirmed the presence of tannins.

Steroids Test

1 mL of aqueous peel extract was added to 2 mL of acetic anhydride in a test tube and then 1.5 mL of H_2SO_4 was added. The violet to blue colour did not appear and confirmed the absence of steroids.

Amino Acid Test

1 mL of aqueous peel extract was mixed with few drops of ninhydrin reagent and no purple colour of solution showed the absence of amino acids.

Reducing Sugar Test

2 mL of aqueous peel extract was added to 0.5 mL of both Fehling's A and B solution and then the mixture was heated in a water bath for 30 minutes. The appearance of brick red colour showed the presence of reducing sugar.

Terpenoids Test

1 mL of aqueous peel extract was mixed to 0.5 mL of H_2SO_4 and 0.5 mL of $CHCl_3$ was added to it. The persistent of reddish-brown colour confirmed the presence of terpenoids.

Cardiac Glycosides Test

4 mL of aqueous peel extract was mixed with glacial acetic acid and then 1 mL of conc. H_2SO_4 was added along with the addition of few drops of $FeCl_3$ into it. The brown colour ring was formed which indicated the presence of cardiac glycosides.

Carbohydrates Test

Molisch's Test: 2 mL of aqueous peel extract was taken in a test tube and few drops of alpha-naphthol was added to it and then few drops of conc. H_2SO_4 was added along with

the side of the test tube. The purple ring appeared which showed the presence of carbohydrates.

Benedict's Test: 1 mL of aqueous peel extract was mixed with 0.5 mL of Benedict's reagent. The characteristic colour of solution appeared that confirmed the presence of carbohydrates.

Phenolics Tests

Ferric Chloride Test: 1 mL aqueous peel extract was mixed with 5 mL of distilled water and 5% of $FeCl_3$. Dark-green colour appeared which showed the presence of phenolics.

Lead Acetate Test: 1 mL of aqueous peel extract was taken and mixed with 3 mL of 10% lead acetate. Bulky white precipitate appeared which showed the presence of phenolics.

Protein test

Biuret Test: 2 ml of aqueous peel extract was mixed with 1 mL of 2% of copper sulphate solution and 1 mL of ethanol and excess of KOH pellets was added to it. The pink colour solution was not formed that confirmed the absence of protein.

Anthraquinone Test

2 mL of aqueous extract was taken in a test tube and 2 mL of 5% KOH was added to it. The pink colour of solution was not formed that showed the absence of anthraquinone.

CHAPTER 4

4. RESULTS AND DISCUSSIONS

4.1 Formation of Iron Oxide (α-Fe_2O_3) Nanoparticles

As depicted in the (figure 4.1a), the addition of 50 mL of *C. maxima* peel extract to a 50 mL solution of 0.1M $FeCl_3.6H_2O$ in a 1:1 ratio resulted in the formation of IONPs, as evidenced by the change in color from yellow to a darker shade (Figure 4.1b). This color change is attributed to the surface plasmon resonance (SPR) phenomenon typically observed in iron oxide nanoparticles and the conversion of Fe^{3+} ions to Fe^0 nanoparticles facilitated by the aqueous *C. maxima* peel extract. The optical absorption spectrum of metal nanoparticles is influenced by factors such as particle size, shape, aggregation state, and the surrounding dielectric medium. Initially, the brown color is primarily attributed to the *C. maxima* peel extract, which gradually fades while undergoing magnetic stirring at 80 °C for 1 hour, resulting in a darker color as the concentration of IONPs increases. To maintain an appropriate pH for IONPs synthesis, the reaction mixture was adjusted to pH 11 using 1M NaOH, monitored by a pH meter, and confirmed by observing the absorbance of IONPs using a UV-visible spectrophotometer (Bhuiyan *et al.*, 2020; Mahlaule-Glory *et al.*, 2022; Adhikari *et al.*, 2022).

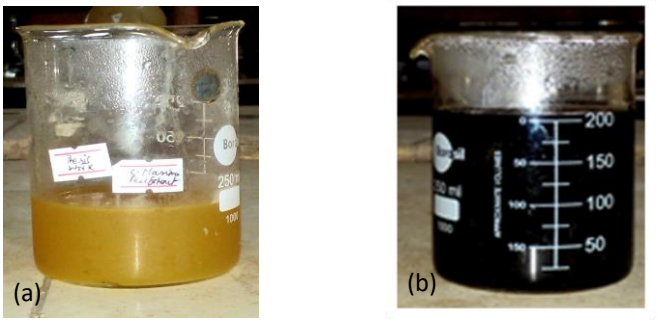

Figure 4.1: (a) & (b) *C. maxima* peel extract and synthesized IONPs.

4.2 Analysis of Optical Properties of IONPs by UV-visible Spectroscopy

Based on the UV-visible spectra provided in figure 4.2, the presence of a distinctive UV absorption peaks at 337 nm and 353 nm at pH 11 confirms the formation of IONPs. Among the various IONPs mixtures, the sharp and intense peak observed at pH 11 indicates the presence of a maximum surface plasmon resonance (SPR) band centered at

353 nm. This observation suggests the reduction of Fe^{3+} ions to Fe^{0} nanoparticles and the development of its corresponding SOR band (Somchaidee *et al.*, 2018; Win *et al.*, 2021).

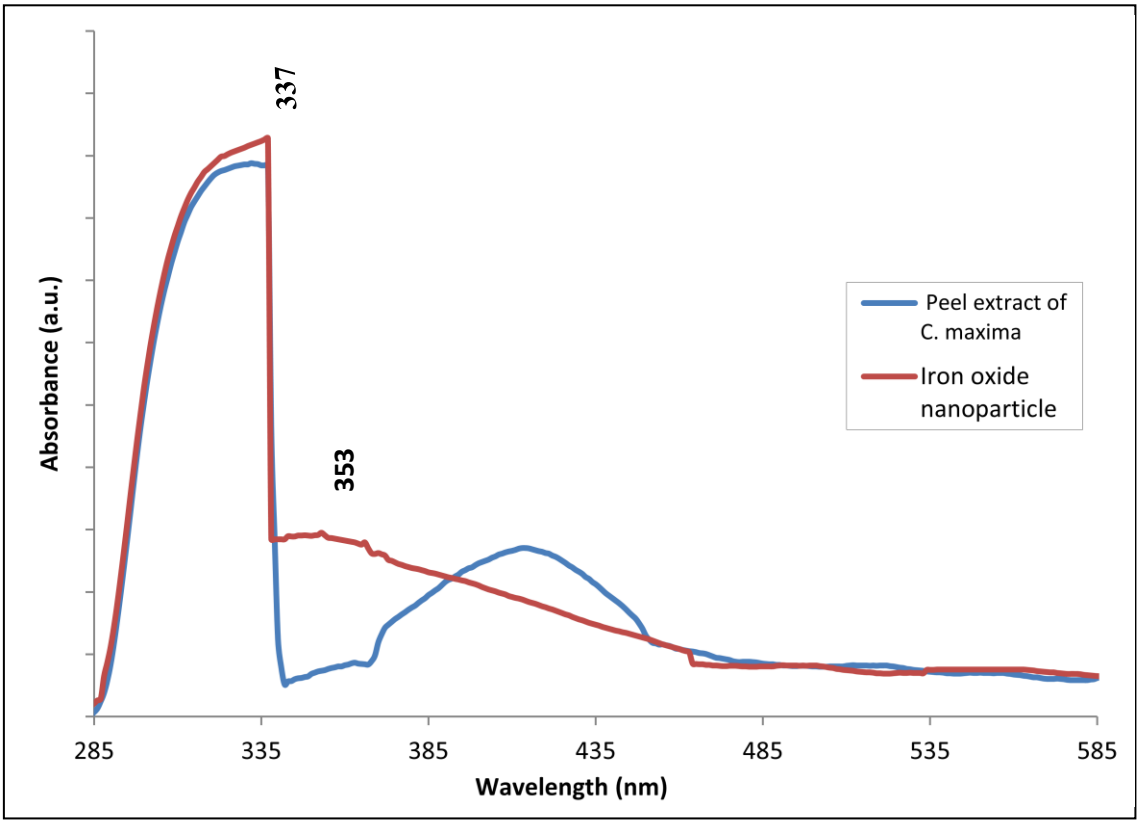

Figure 4.2: UV-visible spectra of IONPs and plant extract.

4.3 FTIR Analysis of *C. maxima* Peel Extract and IONPs

Fourier Transform Infrared Spectroscopy (FTIR) was utilized to detect the functional group present in the plant extract and the resulting nanoparticles. The study revealed that the reaction between phytochemical and metal ions indicated the formation of iron oxide nanoparticles. It was found that the phytochemicals reacted with the iron ions, leading to the formation of the nanoparticles, rather than reducing Fe^{3+} to Fe^{0}. The presence of biomolecules acting as capping agents confirmed the involvement of natural compounds in the synthesis and stability of IONPs. The FTIR analysis of the synthesized sample confirmed the synthesis of IONPs and the presence of various reducing agents, represented by the functional groups present in the *C. maxima* peel extract (Somchaidee *et al.*, 2018; Sundari *et al.*, 2017; Win *et al.*, 2021).

The *C. maxima* peel extract contains various constituents, with polyphenols, naringin, auraptene, naringenin, glycosides and carboxylic acids being primarily responsible for the reduction and stabilization of α-Fe_2O_3 nanoparticles. Polyphenols, in particular, play a

significant role in the reduction process due to their abundant –OH group, which release electrons to conveniently reduce Fe^{3+} to Fe^{0} nanoparticles upon absorption of visible light. During the reduction process, charge transfer occurs, and the initial chelation of Fe^{3+} ions by the aldehyde groups C=O in the *Citrus maxima* peel extract leads to the formation of ferric protein chains (HO-.…Fe^{3+}….) bonds and the subsequent formation of suspended ferric hydroxide $Fe(OH)_3$. Over time, the ferric hydroxide core undergoes dehydration (-H_2O) and transforms into black-colored α-Fe_2O_3 nanoparticles. The protein chain in the *Citrus maxima* peel extract acts as a capping agent on the α-Fe_2O_3 surface through the chelation of COO^{-}……Fe^{3+}. By adjusting the pH to 11 with the addition of 1M NaOH solution to the reaction mixture, any remaining Fe^{3+} ions that were not converted to Fe_2O_3 nanoparticles form suspended ferric hydroxide, $Fe(OH)_3$, contributing to the formation of α-Fe_2O_3 nanoparticles (Adhikari *et al.*, 2022).

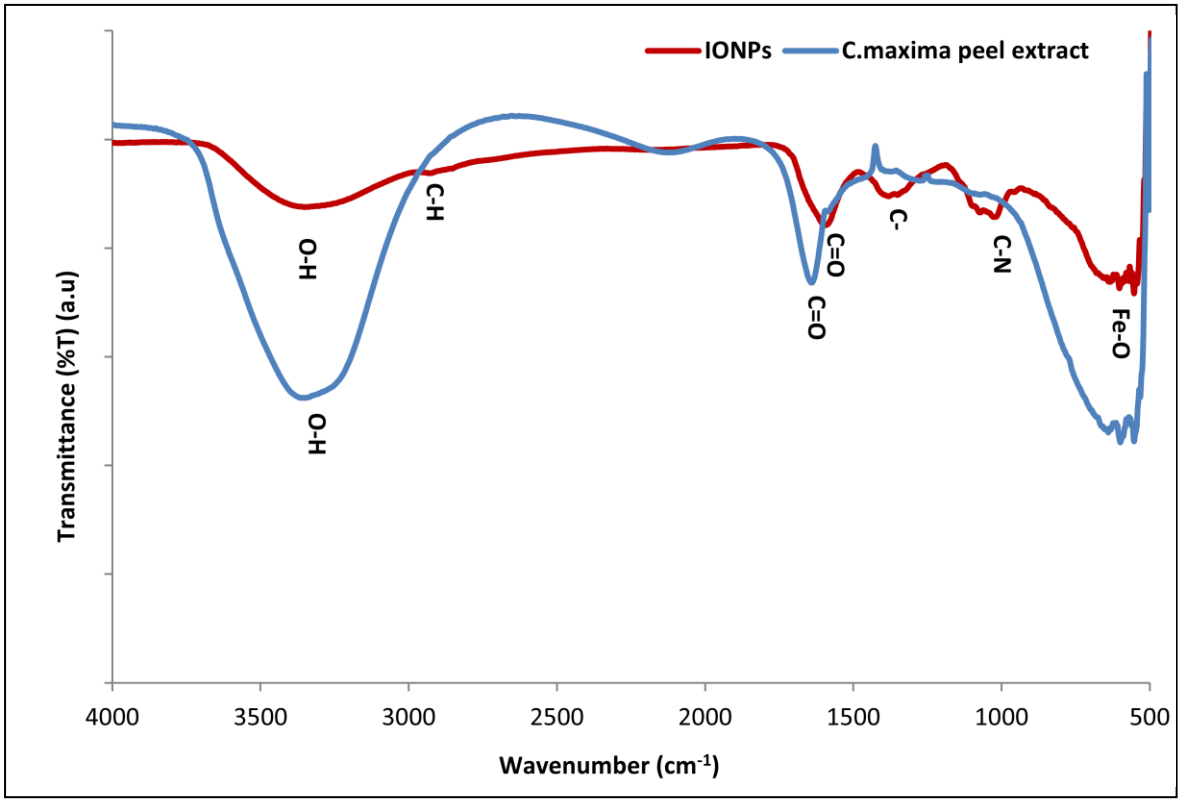

Figure 4.3: FTIR spectra of IONPs and plant extract.

The FTIR spectra of IONPs and *C. maxima* peel extract as shown in figure 4.3 exhibit distinct peaks corresponding to characteristic functional groups at specific wavelengths ranging from (400-4000 cm^{-1}). These functional groups existed in plant extracts act as reducing and stabilizing agents in the nanoparticle synthesis. The peaks observed at 477.28 cm^{-1}, 553.11 cm^{-1} and 639.95 cm^{-1} indicate the presence of Fe-O bond in the sample. The peak observed at 3358.45 cm^{-1} represents O-H bond stretching (H-bonded)

which may be phenolic groups present in polyphenolic compounds. The peak at 2927.58 cm^{-1} is due to the C-H stretching vibration present in fatty acids. Again, the stretching vibration of C=O at 1640.60 cm^{-1} represents the aldehydes and ketones indicating the presence of phenolic acids and terpenoids. The C-O stretching vibration at 1277.58 cm^{-1} suggests the presence of secondary alcohol in the plant extract. Likewise, the peaks observed at 1380.25 cm^{-1} and 1024.07 cm^{-1} represents the C-H bending vibration and C-N stretching vibration respectively indicating the presence of phenols and aliphatic amines. Therefore, the shift in peak position in the range of 400-4000 cm^{-1} suggests that these functional groups containing compounds present in the plant extract are bound to the iron oxide surface (Bhuiyan *et al.*, 2020; Mahlaule-Glory *et al.*, 2022; Adhikari *et al.*, 2022).

4.4 Study of Crystal Structure of IONPs by X-Ray Diffraction

The analysis of the X-ray diffraction (XRD pattern reveals distinct peaks at specific 2θ values: 31.63°, 45.52°, 56.47°, 75.44° and 83.98° corresponding to the lattice plane values of (311), (400), (511), (440) and (533), respectively (Figure 4.4). These peak positions indicate the cubic crystalline structure of the synthesized IONPs, which aligns with the standard JCPDS card number 00-019-0629.

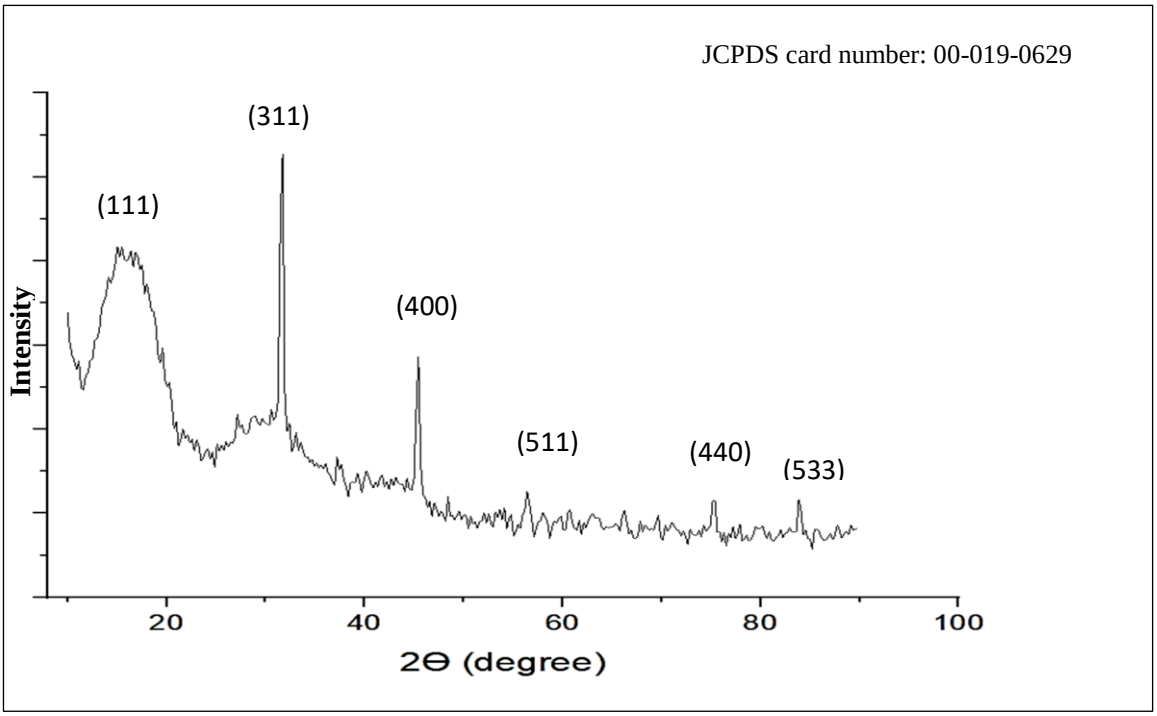

Figure 4.4: XRD pattern of biosynthesized IONPs.

Therefore, based on the XRD pattern, it is confirmed that the IONPs synthesized with the assistance of *C. maxima* are crystalline. These finding are consistent with previously

reported results (Qasim *et al.*, 2020; Somchaidee *et al.*, 2018). Furthermore, utilizing the Scherrer equation and the full width at half maximum (FWHM) value, the average crystallite size was calculated to be 8.70 nm (Adhikari *et al.*, 2022; Somchaidee *et al.*, 2018).

2θ (degree)	**FWHM(degree)**	**Θ (Radians)**	**FWHM (Radians)**	**Size (nm)**	**Average size (nm)**
31.63	0.6278	0.2761	0.01096	12.7155	8.70
45.52	0.6106	0.3972	0.01066	12.5306	
56.47	1.0956	0.4928	0.01912	6.6725	
75.44	0.7824	0.6583	0.01366	8.3886	
83.98	1.9437	0.7329	0.03392	3.1728	

Table 1: Estimation of average size of IONPs.

In addition to these, there are additional smaller peaks observed in the XRD pattern, which could be attributed to the presence of the crystalline bio-organic phase (capping agent) on the surface of the IONPs. It is also possible that these characteristic peaks arise from the partial oxidation of iron, resulting in the observed features.

4.5 Phytochemicals Present in *C. maxima* Peel Extract

The *Citrus maxima* peel extract contains significant amounts of phenolic acids, alkaloids, flavonoids, rutin, coumarin, glycosides, terpenoids, etc (Figure 4.5 a & b) which exhibits anti-diabetic, anti-microbial, anti-inflammatory, anti-cancer, anti-ulcer and hepatoprotective properties used in traditional herbal medicines to cure fever, gout, arthritis, kidney disorders and ulcers.

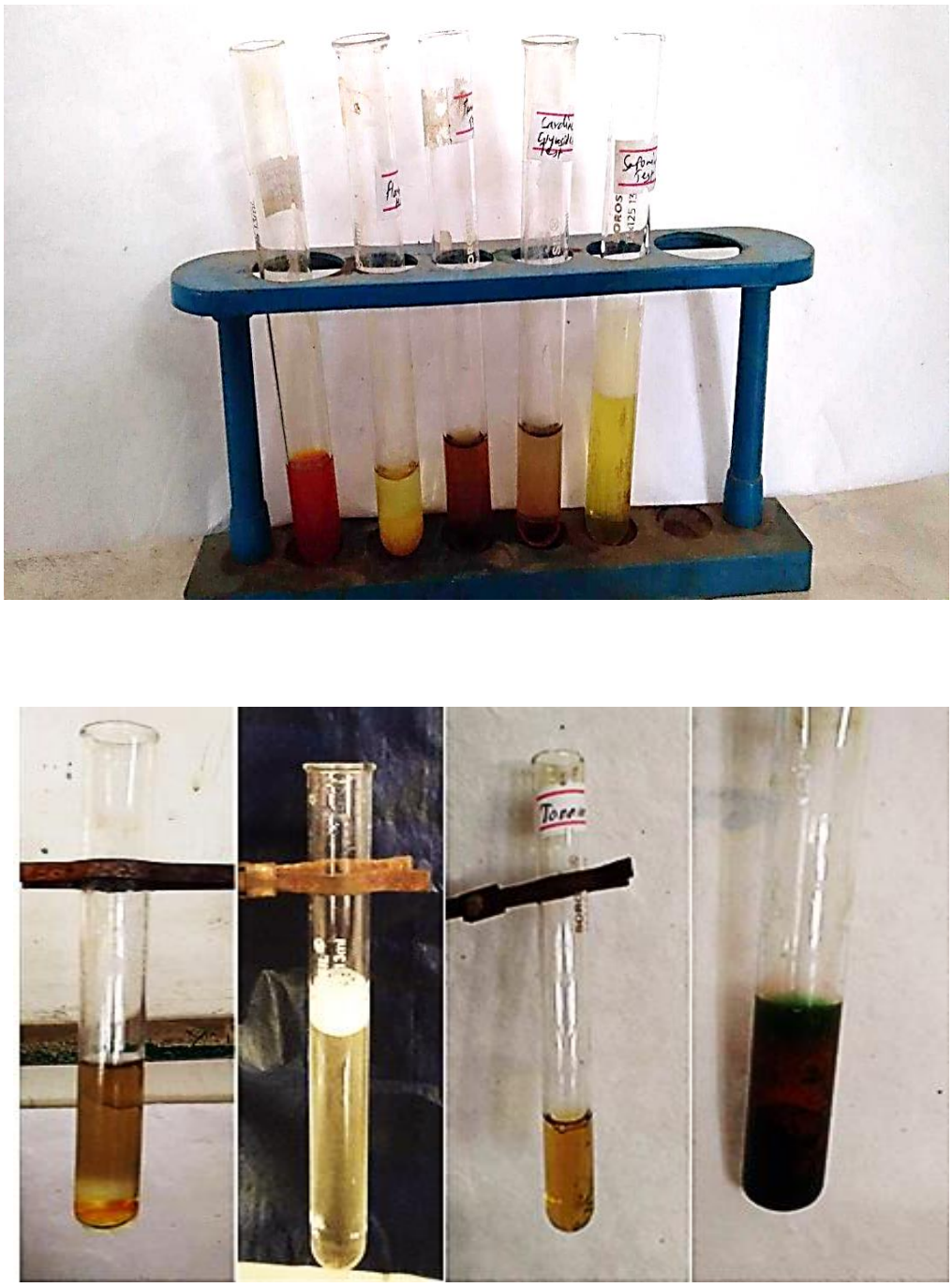

Figure 4.5: Phytochemical analysis of *C. maxima* peel extract.

S.N.	Tests	Inferences
		Aqueous Extract
1.	Alkaloids	+
2.	Flavonoids	+
3.	Saponins	+
4.	Tannins	+
5.	Amino Acids	-
6.	Terpenoids	+
7.	Steroids	-
8.	Reducing Sugars	+
9.	Cardiac Glycosides	+
10.	Carbohydrates	+
11.	Phenolics	+
12.	Proteins	-
13.	Anthraquinones	-

(+) represents the presence of phytochemicals and (-) represents the absence of phytochemicals.

Table 2: Phytochemicals present in *C. maxima* peel extract.

Therefore, the flavonoids present in *C. maxima* peel can convert Fe^{3+} ions into metallic Fe^{0} which functions reducing as well as capping agent to create IONPs. Additionally, the use of other phytochemicals is possible to create films that are anti-microbial and antioxidant used in medicine or food packaging (Zou *et al.*, 2016).

4.6 Degradation of Methylene Blue

The *C. maxima* mediated IONPs were used for the degradation of methylene blue and the process is described in detail. The accompanying image (Figure 4.6) clearly illustrates the change in color of methylene blue at different concentrations upon the addition of IONPs. Specifically, the color of the 10 ppm methylene blue solution shifts to a greenish-blue hue after the introduction of IONPs. This alteration in color indicates a modification in the localized surface plasmon resonance (LSPR) properties of the IONPs, resulting from the interaction between electromagnetic radiation and the electrons on the surface of the nanoparticles (Shahwan *et al.*, 2011). To further analyze the resulting solution, the

absorbance of the 10 ppm methylene blue solution, as well as the mixture of methylene blue and IONPs, was measured using a UV-visible spectrophotometer at wavelengths ranging from 200 nm to 800 nm. The measurements were taken at different time intervals, initially at T0 in dark conditions and subsequently upon exposure to sunlight. The corresponding spectra recorded and analyzed.

Figure 4.6: Photocatalytic degradation of 10 ppm Methylene blue by plant-mediated synthesized IONPs.

4.7 Photocatalytic Degradation of Methylene Blue

The methylene blue of 10 ppm concentration has intense blue color before adding IONPs and H_2O_2. After the addition of 0.2 mL H_2O_2 and 10 mg of IONPs to the MB solution, the blue color of the solution fades away to some extent and degrade photocatalytically (Adhikari *et al.*, 2022). After 90 minutes, it became a colorless solution as shown in the figure 4.7. The objective of this experiment was to assess the effectiveness of synthesized IONPs for the oxidative degradation of methylene blue. The UV-vis spectrum of the MB solution, in the presence of IONPs and H_2O_2, was recorded at various time intervals (e.g., 10 mins, 20 mins, 30 mins, etc up to 90 mins) while continuously stirring on a magnetic

Figure 4.7: Photographic image of the MB dye degradation photocatalytically at different intervals of time by plant-mediated synthesized IONPs.

stirrer in sunlight. To measure the absorbance of the solution, small samples were taken at specific time intervals. Initially, the SPR band of MB was observed at 664 nm with an absorbance of 0.594 nm accompanied by a hump at 620 nm, which is attributed to $\pi \rightarrow \pi^*$ and $n \rightarrow \pi^*$ transitions. Over time, the SPR band gradually decreased from its maximum value of 0.594 at 664 nm due to continuous exposure to sunlight, resulting in a fading of the intense blue color of MB. The decline in the SPR band of the solution, as depicted in

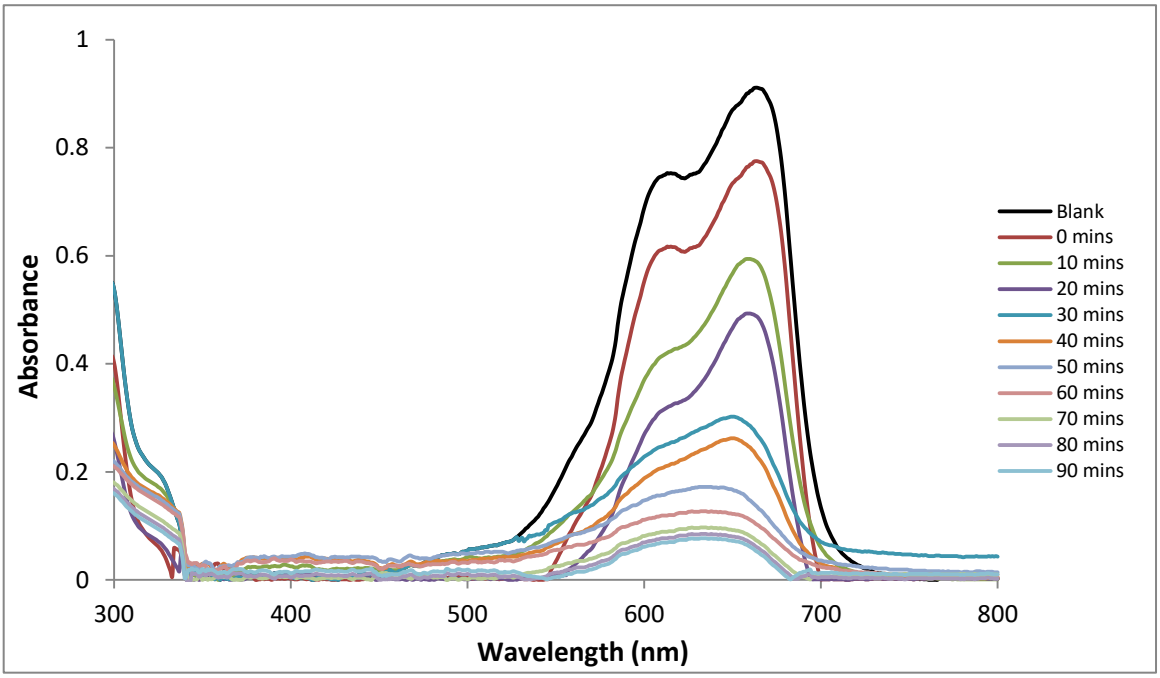

Figure 4.8: Photocatalytic degradation of Methylene blue at different intervals of time by plant-mediated synthesized IONPs taking an amount of 5 mg nanoparticles

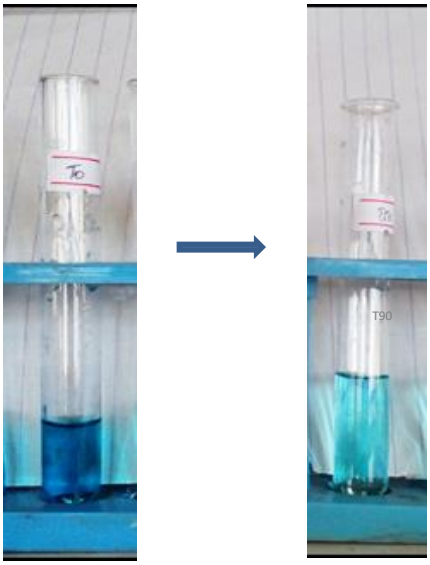

Figure 4.9: Photographic image of the MB dye degradation photocatalytically at different intervals of time by plant-mediated synthesized IONPs of 5mg catalyst loading.

The absorbance of MB at a time zero (A_0) = 0.775		
Time (mins)	**Absorbance at time t (A_t) (nm)**	**Degradation Efficiency (%)**
10	0.622	19.74
20	0.514	33.67
30	0.426	45.03
40	0.336	56.64
50	0.252	67.48
60	0.183	76.38
70	0.119	84.64
80	0.096	87.61
90	0.077	90.06

Table 3: Degradation efficiency estimation of the 5 mg IONPs.

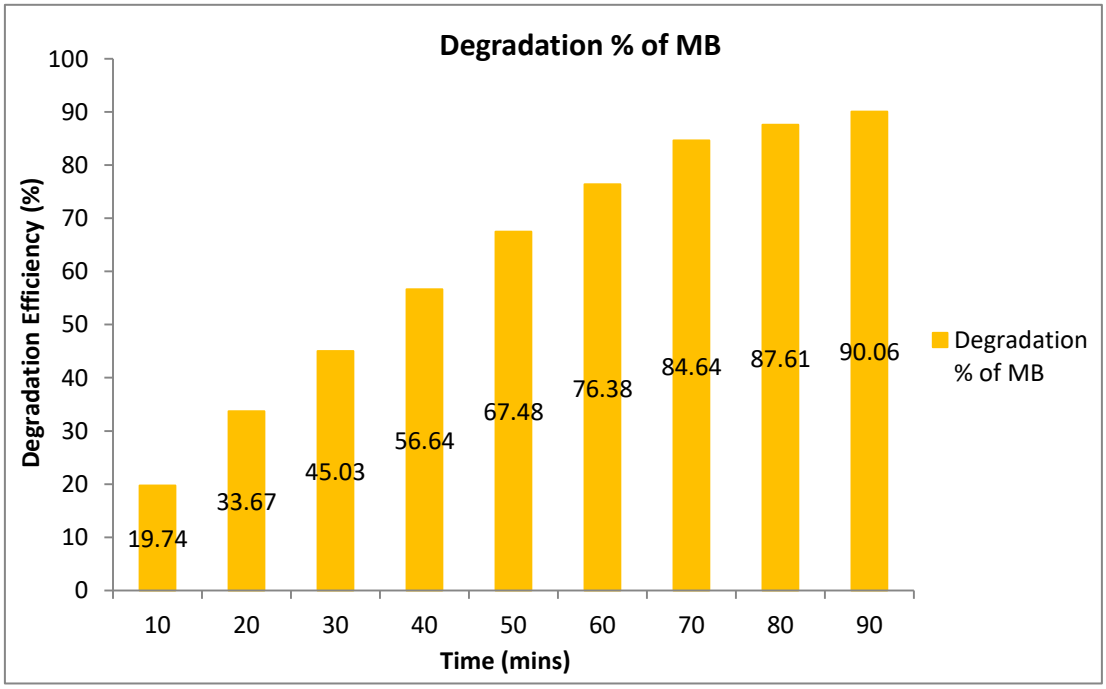

Figure 4.10: Graphical representation of degradation of Methylene blue by 5 mg IONPs.

the figure 4.7, continued until 1.5 hours, and eventually, the solution became colorless after 1.5 hours. The complete degradation of MB was confirmed by the UV-visible spectrophotometer, which exhibited an intense peak at 664 nm. The degradation efficiency of the dye was calculated using the following formula:

$$\text{Efficiency (\%)} = (A_0 - A_t) / A_0 \times 100$$

Where, efficiency (**%**) represents the degradation efficiency of the dye, $\mathbf{A_0}$ corresponds to the absorbance of the dye solution at the beginning (zero time), and $\mathbf{A_t}$ represents the absorbance of the dye solution in suspension after time t. The reactions involved in the degradation process are as follows:

$Fe^{2+} + H_2O_2 \rightarrow \bullet OH + Fe^{3+} + OH^-$ ——————— (i)

$Fe^{3+} + H_2O_2 \rightarrow Fe^{2+} + OOH^{\bullet} + H^+$ ——————— (ii)

$Fe^{2+} + OH\bullet \rightarrow Fe^{3+} + OH^-$ ——————— (iii)

$H_2O_2 + hv \rightarrow OH\bullet + OH^-$ ——————— (iv)

$Fe^{3+} + H_2O + hv \rightarrow Fe^{2+} + \bullet OH + H^+$ ——————— (v)

Equations (i) and (ii) demonstrate that the reaction is initiated by ferrous ions, resulting in the generation of hydroxyl radicals that attack and degrade MB. These hydroxyl radicals also target the bonds in MB whether they are in solution or adsorbed on the surface of IONPs. Previous literatures (Shafreen *et al.*, 2017; Wanakai *et al.*, 2019) indicates that H_2O_2 alone does not cause significant degradation. However, when IONPs are combined with H_2O_2, the color of MB disappears with an efficiency of 90.06%, 98.31% and 93.08% for 5 mg, 10 mg and 20 mg of IONPs respectively, after 90 minutes (Table 1). No significant changes are observed beyond 90 minutes. Incubating MB in an aqueous solution of IONPs and H_2O_2 for 5 minutes results in a red shift of the spectral band from 620 nm to 664 nm, which can be attributed to MB protonation (Shahwan *et al.*, 2011).

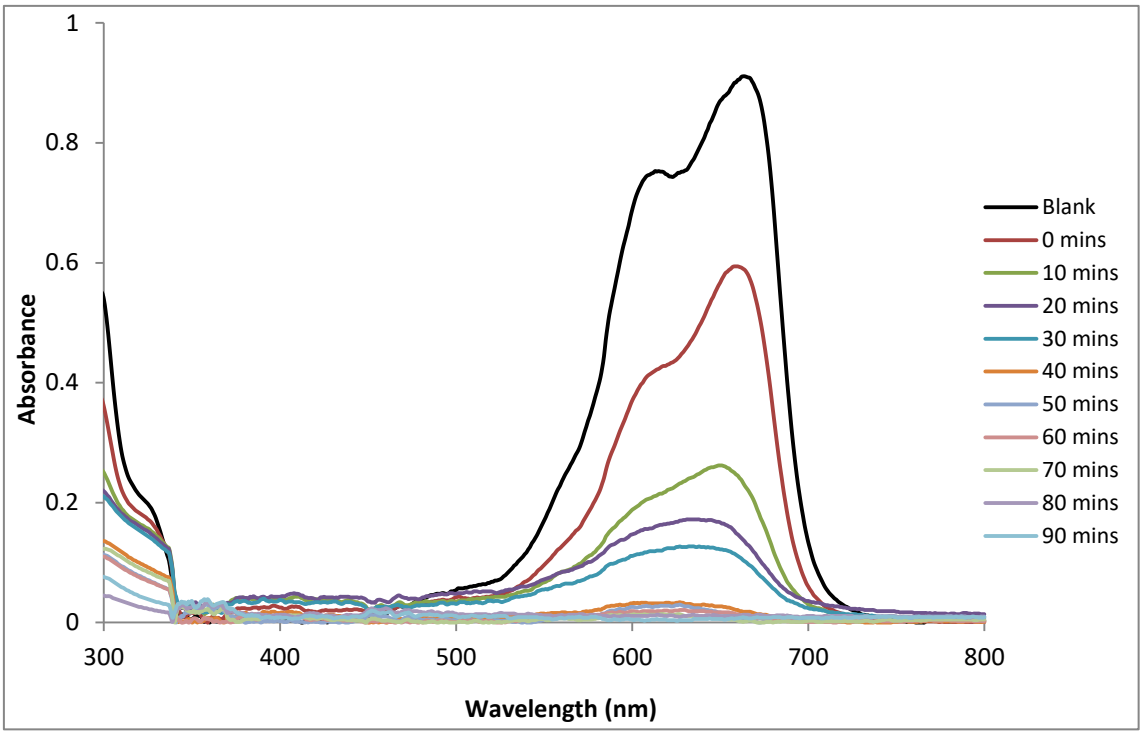

Figure 4.11: Photocatalytic degradation of Methylene blue at different intervals of time by plant-mediated synthesized IONPs taking an amount of 10 mg nanoparticles

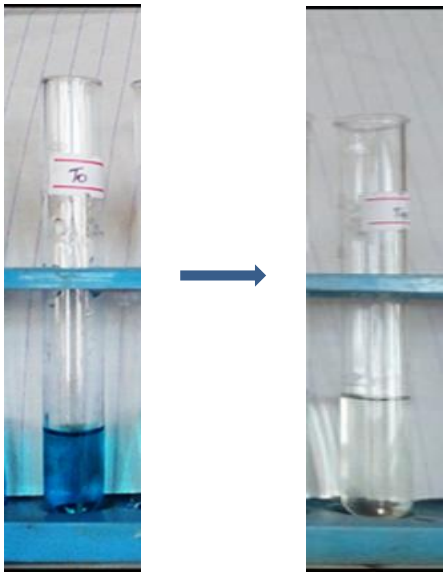

Figure 4.12: Photographic image of the MB dye degradation photocatalytically at different intervals of time by plant-mediated synthesized IONPs of 10mg catalyst loading.

The absorbance of MB at a time zero (A_0) = 0.594		
Time (min)	**Absorbance at time t (At) (nm)**	**Degradation efficiency (%)**
10	0.462	22.22
20	0.372	37.37
30	0.299	49.66
40	0.233	60.77
50	0.169	71.54
60	0.116	80.47
70	0.079	86.70
80	0.041	93.09
90	0.01	98.31

Table 4: Degradation efficiency estimation of the 10 mg IONPs.

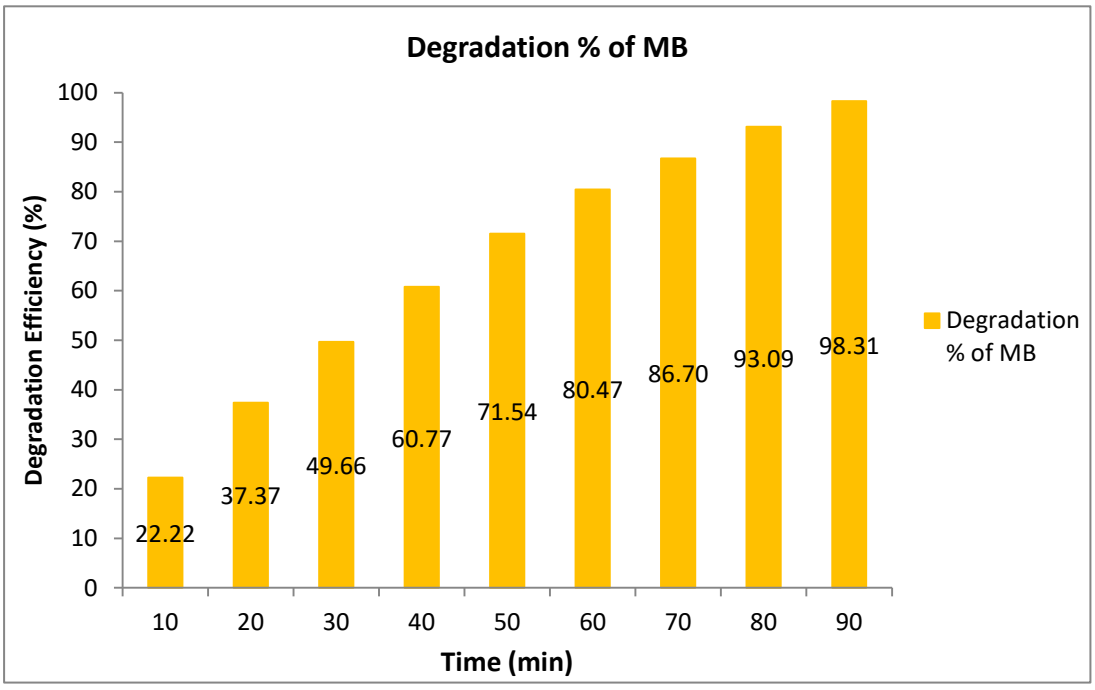

Figure 4.13: Graphical representation of degradation of methylene blue by 10 mg of IONPS.

Consequently, MB undergoes oxidation and decolorization through a Fenton-like reaction, facilitated by IONPs providing ferrous ions. Similar findings have been reported by Adhikari *et al.* (2022), who synthesized IONPs using the sol-gel method and have demonstrated the potential of green-synthesized IONPs for organic dye degradation.

Therefore, the synthesized IONPs can be utilized as heterogeneous Fenton-like oxidants for the degradation of MB in an aqueous medium.

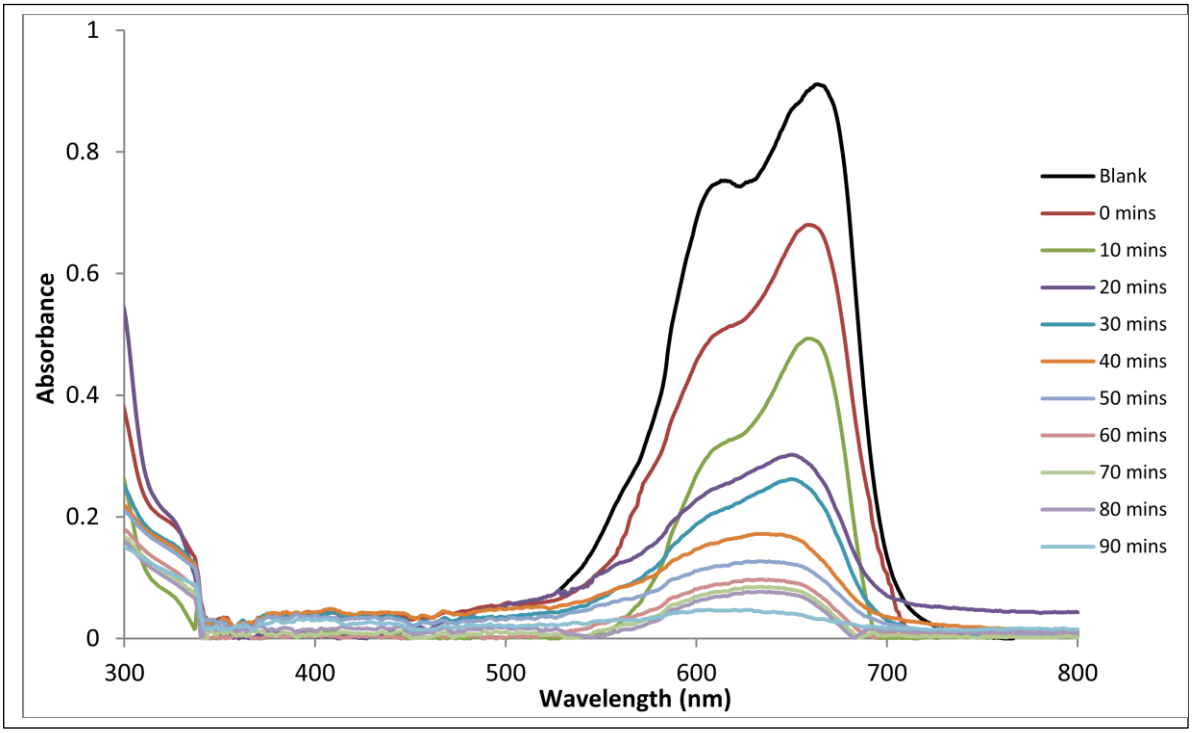

Figure 4.14: Photocatalytic degradation of Methylene blue at different intervals of time by plant-mediated synthesized IONPs taking an amount of 20 mg nanoparticles.

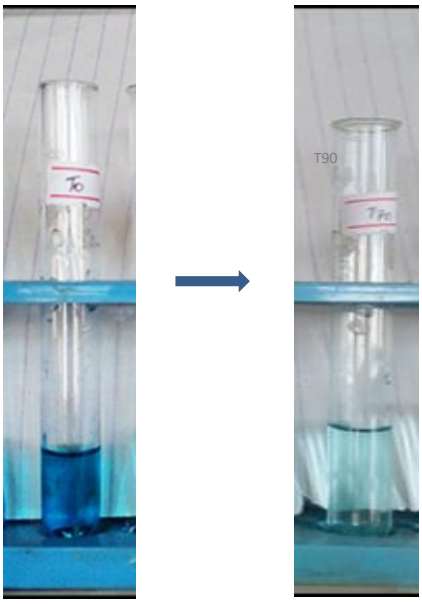

Figure 4.15: Photographic image of the MB dye degradation photocatalytically at different intervals of time by plant-mediated synthesized IONPs of 20 mg catalyst loading.

The absorbance of MB at a time zero (A_0) = 0.680		
Time (mins)	**Absorbance at time t (At) (nm)**	**Degradation Efficiency (%)**
10	0.542	20.29
20	0.432	36.47
30	0.336	50.58
40	0.252	62.94
50	0.186	72.64
60	0.144	78.82
70	0.115	83.08
80	0.077	88.67
90	0.047	93.08

Table 5: Degradation efficiency estimation of the 20 mg IONPs.

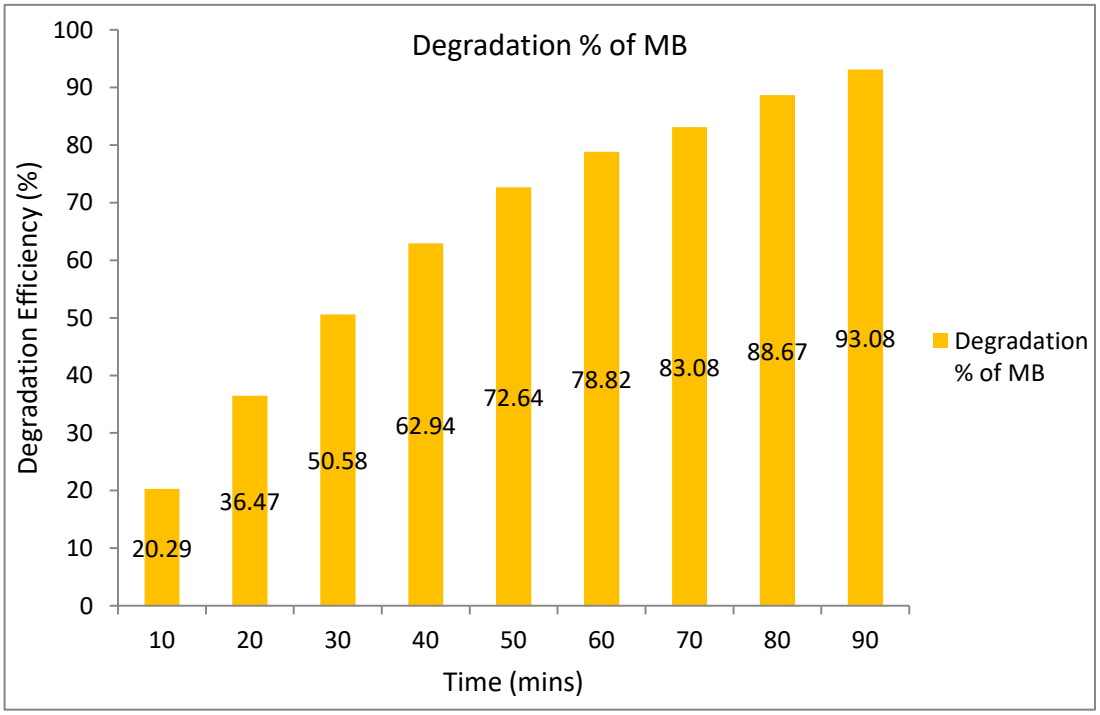

Figure 4.16: Graphical representation of degradation of Methylene blue by 20 mg IONPs.

4.8 Degradation Kinetics of Methylene Blue

The estimation of dye photodegradation's kinetic constants is commonly done by utilizing equations that represent pseudo-first-order and second-order reaction rates (Eq. (vi) and (vii)). The equations for the reaction rate are as follows:

$$\ln(A_0/A_t) = K_1 t \quad \text{..... (vi)}$$

$$1/A_0 - 1/A_t = K_2 t \quad \text{..... (vii)}$$

In these equations, t represents the reaction time in minutes, A_0 is the initial concentration, A_t is the concentration at time t, and K_1 (hr^{-1}) represents the first-order reaction rate constant. The rate constant (K) of the first-order reaction is determined by plotting $\ln(A_0/A_t)$ against the reaction time, t. The slowest degradation rate was observed at 30 minutes for a sample, with a rate constant of 0.00634 min^{-1}, 0.0151 min^{-1} and 0.02751 min^{-1} for 5 mg, 10 mg and 20 mg of IONPs, respectively. This rate increased to 0.01172 min^{-1}, 0.0185 min^{-1} & 0.03157 min^{-1} for 5 mg, 10 mg and 20 mg of IONPs at 90 minutes due to redox reactions occurring between IONPs (Iron Oxide Nanoparticles) and MB (Methylene Blue), resulting in the generation of oxidative free radicals that bind with photocatalysts and trap the molecules of MB, ultimately removing them from polluted water. This indicates that the reaction rate is significantly higher at different time intervals with a slope of 0.01172 min^{-1}, 0.0185 min^{-1} and 0.03157 min^{-1} for 5 mg, 10 mg and 20 mg of IONPs, respectively. The dye degradation reached half of its initial value within 45 minutes, corresponding to a reaction rate of 0.00922 min^{-1}, 0.01298 min^{-1} and 0.03626 min^{-1} for 5 mg, 10 mg and 20 mg of IONPs, respectively. The relative degradation kinetics of IONPs has been reported in published researches (Bhuiyan *et al.*, 2020; Adhikari *et al.*, 2022). Ultimately, within 90 minutes, 90.06%, 98.31% and 93.08% of MB dye degradation was achieved using 5mg, 10 mg and 20 mg of IONPs which continuously produce hydroxyl radicals (OH^-) under sunlight radiation, along with H_2O_2. These compounds are responsible for the degradation of the MB dye and a probable degradation percentage is given in the figure (4.10), (4.13) and (4.16).

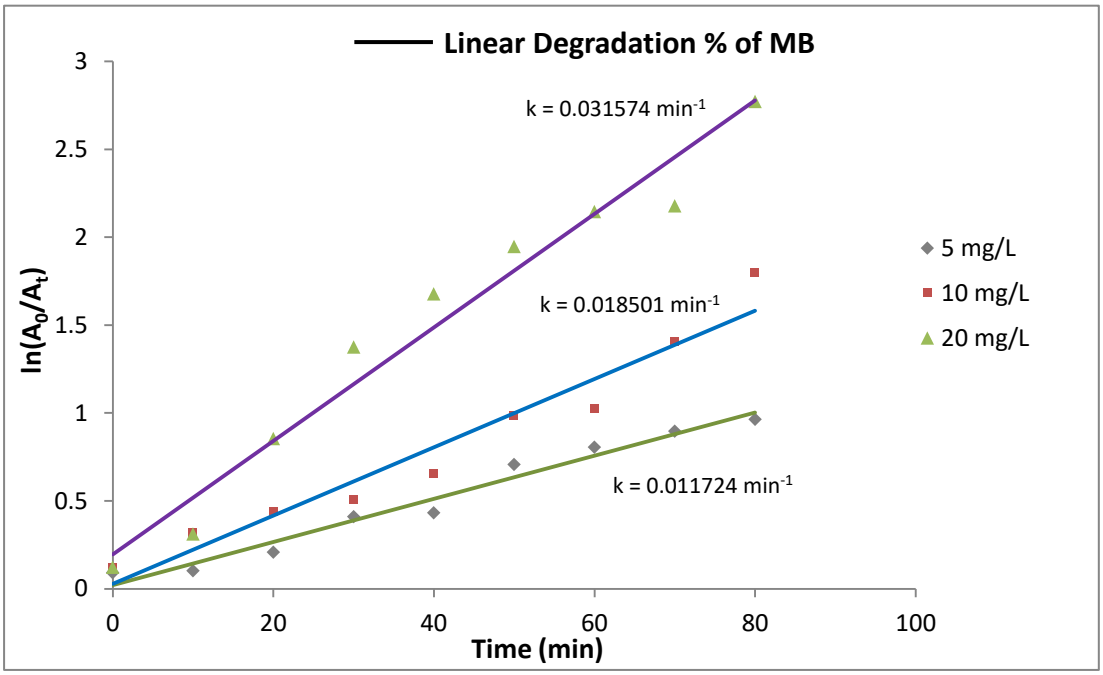

Figure 4.17: The rate of degradation of Methylene Blue by (5 mg, 10mg & 20 mg) of IONPs at different time intervals.

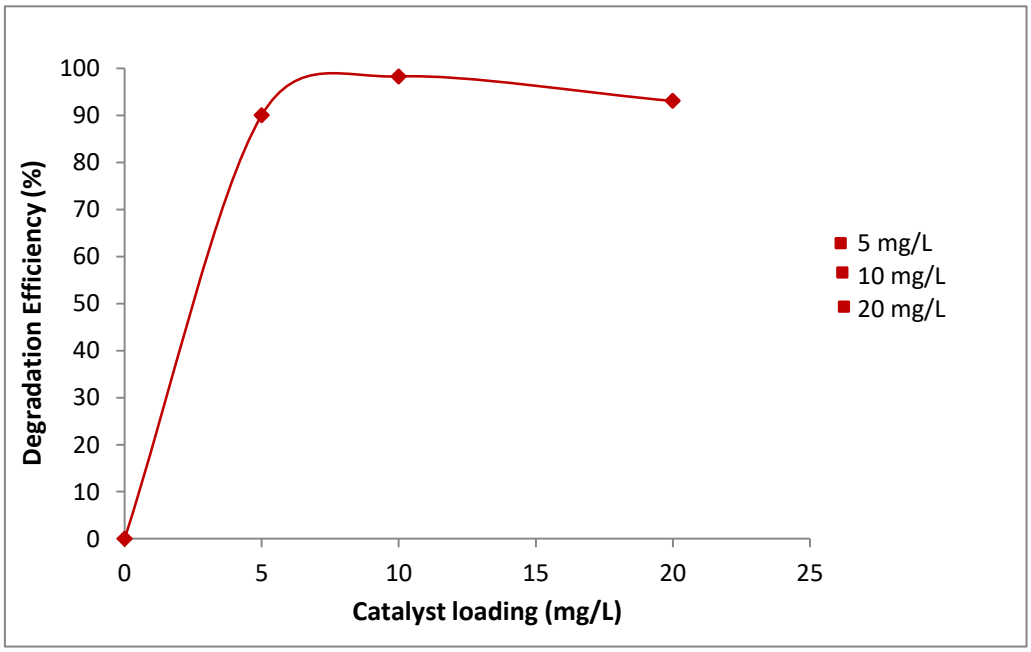

Figure 4.18: The degradation efficiency of Methylene Blue by varying amounts of catalyst (5 mg, 10mg & 20 mg) of IONPs.

In general, when nanoparticles (NPs) are irradiated by sunlight, an electron (e^-) and a hole (h^+) pair are generated (Varadavenkatesan *et al.*, 2019). The electron is excited from the valence band to the conduction band, leaving the hole (H^+) in the valence band. These holes are responsible for the conversion of water into hydroxyl radicals, which then oxidatively degrade the dye. On the other hand, the electron combines with molecular

oxygen to form a superoxide radical. The superoxide radical further converts into a hydroxyl radical, a strong oxidizing agent that degrades the dye into harmless end products (Kamaraj *et al.*, 2019). Additionally, the highly oxidizing holes generated by NPs, after absorbing sunlight, directly oxidize the dyes and release H^+ ions, which then combine with water to produce reactive oxygen species and OH^- ions. These species contribute to the degradation of the dye. Furthermore, the various biomolecules present in plant extract and even in the NPs surface act like catalysts to boost the photocatalytic activity and the subsequent enriched degradation of dye molecules (Haritha *et al.*, 2016).

4.9 Anti-microbial Activity of IONPs

The disc diffusion method was used to investigate the antibacterial effects of IONPs against both Gram-positive (*Bacillus subtilis*) and Gram-negative (*Escherichia coli*) bacteria. The IONPs synthesized through biosynthesis exhibited superior antibacterial activity, as evidenced by larger zones of inhibition, against *B. subtilis* and *E. coli*. A comparison between *B. subtilis* and *E. coli* demonstrated that the green-synthesized IONPs displayed effective antibacterial activity, with a zone of inhibition measuring 15 mm for *B. subtilis* and 7 mm for *E. coli* (Figure 4.19 a,b and 4.20 a). These findings suggest that the biosynthesized IONPs can convert dissolved oxygen molecules into superoxide radical anions (O_2^-) (Das *et al.*, 2020; Ismail *et al.*, 2015), resulting in the production of free radicals such as $\cdot O_2$ and OH^-. These radicals can depolymerize polysaccharides, induce DNA strand breaks, initiate lipid peroxidation, and deactivate enzymes, ultimately leading to cell death. Additionally, it is plausible that the interaction between nanoparticles and cell membrane proteins through electrostatic interactions, as well as the accumulation of nanoparticles in the cytoplasm or periplasmic region, disrupts cellular function and causes membrane disruption and disorganization (Rufus *et al.*, 2016).

The antifungal activity of IONPs against *Candida albicans* was evaluated using the Agar Well Disc Diffusion method. The green-synthesized IONPs exhibited notable antifungal activity against *C. albicans*, with a zone of inhibition measuring 6 mm (Figure 4.19 c and 4.20 b). These findings align with previously published results (Seddighi *et al.*, 2017). Previous research has proposed two possible mechanisms for the interaction between nanoparticles and bacteria/fungi. One mechanism involves the increased production of reactive oxygen species (ROS) such as hydroxyl radicals ($OH^{\cdot}$), singlet oxygen ($O_2^{\bullet}$), and

hydrogen peroxide (H_2O_2) (Caldeiro *et al.*, 2021). When IONPs with defects are activated by UV or visible light, electron-hole pairs are formed. The resulting holes can split H_2O molecules into OH^- and H^+. Additionally, the addition of electrons converts dissolved oxygen molecules into superoxide radical anions (O_2). These free radicals are consistent with results reported elsewhere (Das *et al.*, 2020; Rufus *et al.*, 2016).

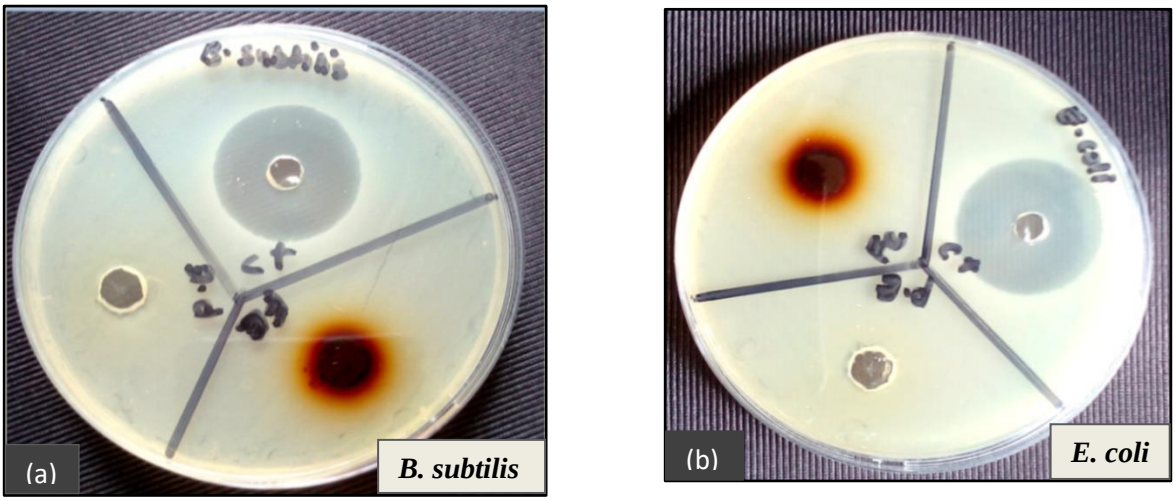

Figure 4.19: (a) and (b) Anti-microbial activity of IONPs against different bacterial strains.

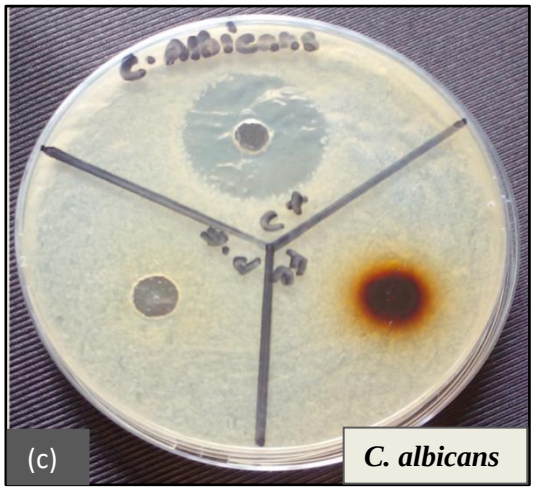

Figure 4.19: (c) Anti-microbial activity of IONPs against fungi.

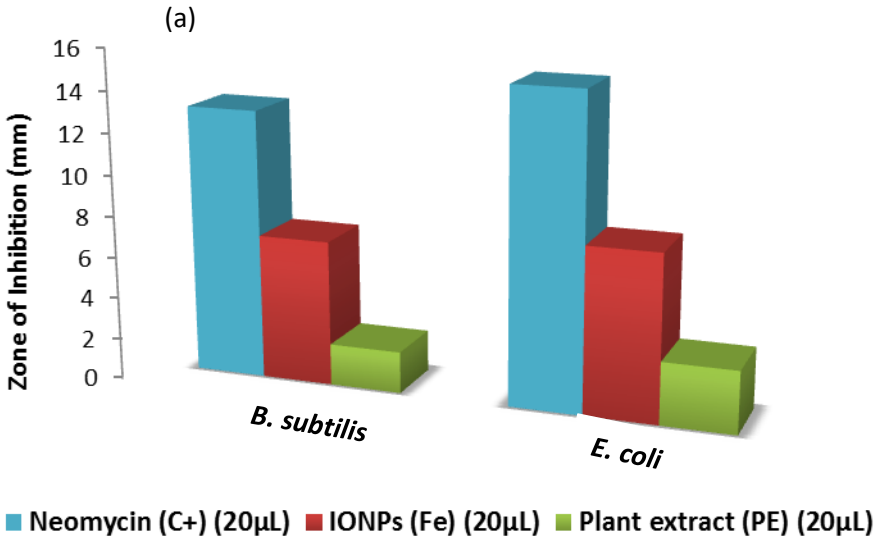

Figure 4.20: (a) Comparative graphical representation of bactericidal inhibition zone of iron oxide nanoparticles on bacterial strains.

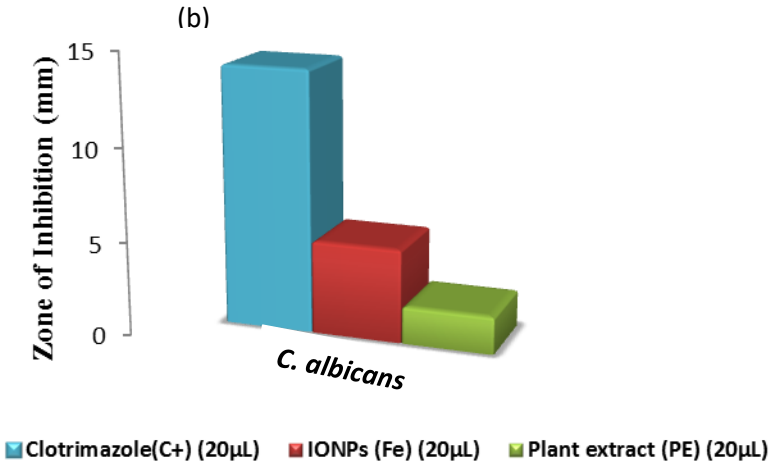

Figure 4.20: (b) Comparative graphical representation of fungicidal inhibition zone of iron oxide nanoparticles on fungal strain.

CHAPTER 5

5. CONCLUSION

Green synthesis of iron oxide nanoparticles using *C. maxima* peel extract was completed and confirmed by the color change and SPR spectra of the solution. The maximum absorption peaks were in the range of 337 and 353 nm in the UV-vis spectra. It was affirmed that the *C. maxima* peel extract has the special property to reduce Fe^{3+} ion to Fe^{0}, the IONPs, and the average size of IONPs was calculated to be 8.70 nm from XRD peaks using Scherrer's equation. FTIR spectra of the as-synthesized IONPs assured that the reducing and capping agents are polyphenolic compounds present in the extract.

The as-synthesized IONPs were found to play a vital role in the degradation of harmful organic dyes like methylene blue from polluted water photocatalytically in 90 minutes with 90.06%, 98.31% and 93.08% efficiency by the dose of 5 mg, 10 mg and 20 mg of IONPs per 100 mL of 10 ppm dye solution, respectively. Such results can be crucial in the field of industry for commercial use. Likewise, in vitro study of the IONPs also demonstrated good anti-bacterial activity against *Bacillus subtilis* and *E. coli* and good anti-fungal activity in vitro against *Candida albicans* demonstrating the way for topical administration against these bacterial and fungal infections. Furthermore, the green synthesis of IONPs using peels of *C. maxima* may be helpful in the field of nanotechnology which has a potential contribution to the field of research and the protection of the environment.

5.1 Future Prospect

The present research work was conducted using the aqueous extract of C. *maxima* peels, which was capable of producing IONPs and was quite stable in solution. The synthesized IONPs showed excellent photocatalytic activity against methylene blue degradation and anti-microbial activity. Hence, different parameters including initial concentration of dye solution, pH of the solution, temperature and the ratios of plant extracts and precursor solution should be considered in future experiments for more efficacy for photocatalytic and anti-microbial applications. Also, several other researches can be conducted in the list below for other potential applications of IONPs in different fields.

- Effect of initial concentration of dye solution, pH of the solution, temperature and the ratios of plant extracts and precursor solution can be studied as the further work of this study.
- Comprehensive study and experimental works can be carried out for the preparation of IONPs for sensing applications.
- For large-scale manufacture, the concentration of the extract and the effect of the temperature on nanoparticles synthesis should be monitored.
- The use of IONPs via greener routes can be employed in various fields of nanotechnology like biomedical, agriculture, catalysis, sensors, environmental protection, water purification and pigments and coatings by detailed study of their reaction mechanisms and effects for the sustainable and clean environment.

REFERENCES

Abd ellah, N. H., & Abouelmagd, S. A. (2017). Surface Functionalization of Polymeric Nanoparticles for Tumor Drug Delivery: Approaches and Challenges. Expert Opinion on Drug Delivery, 14(2), 201-214

Adhikari, A. , Chhetri, K. , Acharya D., Pant, B., & Adhikari, A. (2022). Green Synthesis of Iron Oxide Nanoparticles Using *Psidium guajava* L. Leaves Extract for Degradation of Organic Dyes and Anti-microbial Applications. Catalysts, 12, 1188.

Ahammed, K.R., Ashaduzzaman, M., Paul, S.C. (2020). Microwave Assisted Synthesis of Zinc Oxide (ZnO) nanoparticles in a Noble Approach: Utilization for Antibacterial and Photocatalytic Activity. SN Appl. Sci. 2, 955.

Ahmed, S., Saifullah, Ahmad, M., Swami, B. L., & Ikram, S. (2016).Green Synthesis of Silver Nanoparticles Using *Azadirachta indica* Aqueous Leaf Extract. Journal of Radiation Research and Applied Sciences, 9(1), 1–7.

Akhavan, O., & Azimirad, R. (2009). Photocatalytic Property of Fe_2O_3 Nanograin Chains Coated by TiO_2 Nanolayer in Visible Light Irradiation. Appl. Catal. A Gen.,369,77–82.

Ali, A., Hira Zafar, M. Z., Ul-Haq, I., Phull, A. R., Ali, J. S., & Hussain, A. (2016). Synthesis, Characterization, Applications and Challenges of Iron Oxide Nanoparticles. Nanotech. Sci. Appl., 9 : 49

AlMatar, M., Makky, E.A., Var, I., & Koksal, F. (2018). The Role of Nanoparticles in the Inhibition of Multidrug-Resistant Bacteria and Biofilms. Curr. Drug Deliv., 15, 470-484.

Anchan, S., Pai, S., Sridevi, H., Varadavenkatesan, T., Vinayagam, R., & Selvaraj, R. (2019). Biogenic Synthesis of Ferric Oxide Nanoparticles Using the leaf extract of *Peltophorum pterocarpum* and Their Catalytic Dye Degradation Potential, Biocatal. Agric. Biotechnol. 20, 101251.

Ardakani, L.S., Alimardani, V., Tamaddon, A.M., Amani, A.M., & Taghizadeh, S. (2021). Green Synthesis of Iron-Based Nanoparticles Using *Chlorophytum comosum* Leaf Extract: Methyl Orange Dye Degradation and Antimicrobial Properties. Heliyon,7, e06159.

Astefanei, A., Nunez, O., & Galceran, M. T. (2015). Characterization of Fullerenes: A critical review. Analytica Chimica Acta, 882, 1-21

Bharani, M., Karpagam, T., Badrinarayan, V., Gayathiri, V., & Priya, K. (2013). Synthesis and Characterization of Silver nanoparticles from *Wrightia tinctoria*. International Journal of Applied Biology and Pharmaceutical Technology, 3.

Bhuiyan, M.S.H., Miah, M.Y., Paul, S.C., Das, T. Aka., Saha, O., Rahaman, M.M., Sharif, M.J.I., Habiba, O., & Ashaduzzaman, M. (2020). Green synthesis of Iron Oxide Nanoparticle Using *Carica papaya* Leaf Extract: Application for Photocatalytic Degradation of Remazol Yellow RR dye and Antibacterial Activity, Heliyon 6.

Bibi, I., Nazar, N., Ata, S., Sultan, M., Ali, A., Abbas, A., Jilani, K., Kamal, S., Sarim, F.M., Khan, M.I., Jalal, F., & Iqbal, M. (2019). Green Synthesis of Iron Oxide Nanoparticles Using Pomegranate Seeds Extract and Photocatalytic Activity Evaluation for the Degradation of Textile Dye, J. Mater. Res. Technol. 8 ,6115–6124.

Brown, P. J., & Stevens, K. A. (2007). Nanofibers and Nanotechnology in Textiles. CRC press.

Buzea, C., Pacheco, I. I., & Robbie, K. (2007). Nanomaterials and Nanoparticles: Sources and Toxicity. Biointerphases, 2(4), MR17–MR

Caldeirão, A.C.M., Araujo, H.C., Tomasella, C.M., Sampaio, C., dos Santos Oliveira, M.J., Ramage, G., Pessan, J.P., & Monteiro, D.R. (2021). Effects of Antifungal Carriers Based on Chitosan-Coated Iron Oxide Nanoparticles on Microcosm Biofilms. Antibiotics, 10,588.

Camargo, P. H. C., Satyanarayana, K. G., & Wypych, F. (2009). Nanocomposites: Synthesis, Structure, Properties and New Application Opportunities. Materials Research, 12(1), 1–39

C. Thomas., S. Harshita., Kumar, Mishra, P., & Talegaonkar, S. (2015). Ceramic Nanoparticles: Fabrication Methods and Applications in Drug Delivery. Current Pharmaceutical Design, 21(42), 6165- 6188.

Das, S., Diyali, S., Vinothini, G., Perumalsamy, B., Balakrishnan, G., Ramasamy, T., Dharumadurai, D., & Biswas, B. (2020). Synthesis, Morphological Analysis, Antibacterial Activity of Iron Oxide Nanoparticles and the Cytotoxic Effect on Lung Cancer Cell Line. Heliyon, 6, e04953.

Deraz, N.M., & Abd-Elkader, O.H. (2013). Investigation of Magnesium Ferrite Spinel Solid Solution with Iron-rich Composition. Int. J. Electrochem. Sci. 8, 9071–9081.

Elliott, A., Shibuta, Y., Amara, H., Bichara, C., & Neyts, E. (2013). Atomistic Modeling

of CVD Synthesis of Carbon Nanotubes and Graphene. Nanoscale, 5(15), 6662-6676.

Gang, L., Jinhao, G., Hua, A., & Xiaoyuan, C. (2012). Applications and Potential Toxicity of Magnetic Iron Oxide Nanoparticles. Small, 9(9-10), 1533-1545.

Garrigue, P., Delville, M. H., Labrugere, C., Cloutet, E., Kulesza, P. J., Morand, J. P., & Kuhn, A. (2004). Top-down Approach for the Preparation of Colloidal Carbon Nanoparticles. Chemistry of Materials, 16(16), 2984-2986.

Groiss, S., Selvaraj, R., Varadavenkatesan, T., & Vinayagam, R. (2017). Structural Characterization, Antibacterial and Catalytic Effect of Iron Oxide Nanoparticles Synthesised Using the Leaf Extract of *Cynometra Ramiflora*. J. Mol. Struct. 1128, 572–578

Hamalo-glu, K.€O., Sa_g, E., & Tuncel, A. (2017). Bare, Gold and Silver Nanoparticle Decorated, Monodisperse-porous Titania Microbeads for Photocatalytic Dye Degradation in a Newly Constructed Microfluidic, Photocatalytic Packed-bed Reactor. J. Photochem. Photobiol. Chem. 332, 60–65.

Haritha, E., Roopan, S.M., Madhavi, G., Elango, G., Al-Dhabi, N.A., Arasu, M.V. (2016). Green Chemical Approach Towards the Synthesis of SnO_2 NPs in Argument with Photocatalytic Degradation of Diazo Dye and Its Kinetic Studies. J. Photochem. Photobiol. Biol. 162, 441–447.

Hassan, M.M., & Carr, C.M. (2018). A Critical Review on Recent Advancements of the Removal of Reactive Dyes from Dyehouse Effluent by Ion-exchange Adsorbents. Chemosphere 201–209

Hisatomi, T., Kubota, J., & Domen, K. (2014). Recent Advances in Semiconductors For Photocatalytic and Photoelectrochemical Water Splitting. Chemical Society Reviews, 43(22), 7520-7535.

Immich, A.P.S., Ulson de Souza, A.A., Ulson de Souza S. M., & de, A.G. (2009). Removal Of Remazol Blue RR Dye from Aqueous Solutions with Neem Leaves and Evaluation of their acute toxicity with *Daphnia magna*. J. Hazard Mater. 164,1580–1585.

Izadiyan, Z., Shameli, K., Miyake, M., Hara, H., Mohamad, S.E.B., Kalantari, K., Taib, S.H.M., & Rasouli, E. (2020). Cytotoxicity Assay of Plant-mediated Synthesized Iron Oxide Nanoparticles Using *Juglans regia* Green husk Extract. Arab. J. Chem. 13.

Jain, P. K., El-Sayed, I. H., & EI-Sayed, M. A. (2007). Au Nanoparticles Target

Cancer. Nano Today, 2 (1), 18-29.

Jamzad, M., & Kamari, B. M. (2020). Green Synthesis of Iron Oxide Nanoparticles by the Aqueous Extract of *Laurus Nobilis* L. Leaves and Evaluation of the Antimicrobial Activity. J.Nanostruct. Chem., 10, 193–201.

Jeong, H. H. (2017). Programmable Chiral Nanocolloids.

Kamaraj, M., Kidane, T., Muluken, K.U., Aravind, J. (2019). Biofabrication of Iron Oxide Nanoparticles as a Potential Photocatalyst for Dye Degradation with Antimicrobial Activity. Int. J. Environ. Sci. Technol. 16(5), 8305–8314.

Khandel, P., Yadaw, R. K., Soni, D. K., Kanwar, L., & Shahi, S. K. (2018). Biogenesis of Metal Nanoparticles and Their Pharmacological Applications: Present Status and Application Prospects. Journal of Nanostructure in Chemistry, 8(3), 217 –254.

Kirdat, P. N., Dandge, P.B., Hagwane, R.M., Nikam, A.S., Mahadik, S.P., & Jirange, S.T. (2021). Synthesis and Characterization of Ginger (*Z. officinale*) Extract Mediated Iron Oxide Nanoparticles and Its Antibacterial Activity. Materials Today: Proceedings, 43, 2826-2831.

Kumar, B.; Kumari, S.; Galeasc, S.; Sharmad, V.; Guerreroc, V. H.; Debuta, A.; Cumbala, L. (2020). Characterization and Application of Biosynthesized Iron Oxide Nanoparticles Using *Citrus paradisi* Peel: A Sustainable Approach. Inorganic Chemistry Communications. 119-108116.

Laffon, B., Saquib, Q., Faisal, M., Al-Khedhairy, A., & Alatar, A. (2018). Cellular and Molecular Toxicity of Iron Oxide Nanoparticles. Advances in Experimental Medicine and Biology, vol. 1048. Springer, Cham.

Lateef, A., Asafa, T.B., Beukes, L.S., Hakeem, A.S., & Irshad, H.H. (2020). Multi-functional Titanium Dioxide Nanoparticles Biofabricated via Phytosynthetic Route Using Extracts of *Cola nitida*: Antimicrobial, Dye Degradation, Antioxidant and Anticoagulant Activities, Inorg. Chem. Commun. 6, e04610.

Lin, P.-C., Lin, S., Wang, P. C., & Sridhar, R. (2014). Techniques for Physicochemical Characterization of Nanomaterials. Biotechnology Advances, 32(4), 711–726.

Mahlaule-Glory, L. M., Mapetla, S., Makofane, A., Mathipa, M. M., & Hintsho-Mbita, N.C. (2022). Biosynthesis of Iron Oxide Nanoparticles for the Degradation of Methylene Blue Dye, Sulfisoxazole Antibiotic and Removal of Bacteria fromReal Water. Heliyon, 8, e10536.

Maxim, A., Abakumov., Alevtina, S. S., Alexandar, S. S., Daniil, A. V., Anna, V.,

Elena, M., Galina, A. D., Alexander, G. M., & Vladimir, P. C. (2018). Journal of Biochemical and Molecular Toxicology, 32(12), e22225.

Muthukumar, H., Mohammed, S.N., Chandrasekaran, N.I., Sekar, A.D., Pugazhendhi, A., & Matheswaran, M., (2018). Effect of Iron doped Zinc Oxide Nanoparticles Coating in the Anode on Current Generation in Microbial Electrochemical Cells. Int. J. Hydrogen Energy 44, 2407–2416.

Narayan, N., Meiyazhagan, A., & Vajtai, R. (2019). Metal Nanoparticles as Green Catalysts. Materials, 12, 3602.

Naseem, T., & Durrani, T. (2021). The Role of Some Important Metal Oxide Nanoparticles for Wastewater and Antibacterial Applications. A Review. Environ. Chem. Ecotoxicol., 3, 59–75.

Ohring, M. (2001). The Materials Science of Thin Films. Deposition and Structure (2^{nd} edition) 742.

Priyadarshana, G., Kottegoda, N., Senaratne, A., Alwis, A. de., & Karunaratne, V. (2016). Synthesis of Magnetite Nanoparticles by Top-down Approach from a High Purity ore. Journal of Nanomaterials,16(1), 317:317.

Puri, A., Loomis, K., Smith, B., Lee, J. H., Yavlovich, A., Heldman, E., & Blumenthal, R. (2009). Lipid-Based nanoparticles as Pharmaceutical Drug Carriers: From Concepts to Clinic. Critical Reviews & Trade; in Therapeutic Drug Carrier Systems, 26(6).

Qasim, S., Zafara, A., Muhammad Saqib, S., Alib, Z., Nazara, M., Muhammad Waqasa., Ul-Haqa, A.,Tariqa, T., Hassand, S. G., Iqbalc, F., Shue, X-Gang., & Hasana, M. (2020). Green Synthesis of Iron Oxide Nanorods Using *Withania coagulans* Extract Improved Photocatalytic Degradation and Antimicrobial Activity. Journal of Photochemistry & Photobiology, B: Biology 204 (2020), 111784

Rajeshkumar, S., & Bharath, L. V. (2017). Mechanism of Plant-mediated Synthesis of Silver Nanoparticles – A review on Biomolecules Involved, Characterisation and Antibacterial Activity. Chemico-Biological Interactions, 273, 219–227.

Rufus, A., Sreeju, N., & Philip, D. (2016). Synthesis of Biogenic Hematite (_-Fe_2O_3) Nanoparticles for Antibacterial and Nanofluid Applications. RSC Adv., 6, 94206 –94217.

Samrot, A.V., Rashmitha, S., Veera, P., Sahithya, C.S. (2018). *Azadirachta indica* Influenced Biosynthesis of Super-paramagnetic Iron-oxide Nanoparticles and Their Applications in Tannery Water Treatment and X-ray Imaging. J. Nanostructure Chem. 8, 343–351

Seddighi, N.S., Salari, S., & Izadi, A.R. (2017). Evaluation of Antifungal Effect of Iron Oxide Nanoparticles Against Different *Candida* Species. IET Nanobiotechnol., 11, 883.

Shafreen, R.B., Seema, S., Ahamed, A.P., Thajuddin, N., & Alharbi, S.A. (2017). Inhibitory Effect of Biosynthesized Silver Nanoparticles From Extract of *Nitzschia palea* Against Curlimediated Biofilm of *Escherichia coli*, Appl. Biochem. Biotechnol. 183, 1351-1361.

Shahwan, T., Abu Sirriah, S., Nairat, M., Boyac, E., Ero˘ glu, A.E., Scott,T.B., & Hallam, K.R. (2011). Green Synthesis of Iron Nanoparticles and Their Application as a Fenton-like Catalyst for the Degradation of Aqueous Cationic and Anionic Dyes. Chem. Eng. J., 172, 258–266.

Somchaidee, P., & Tedsree, K. (2018). Green Synthesis of High Dispersion and Narrow Size Distribution of Zero-Valent Iron Nanoparticles Using Guava Leaf (*Psidium Guajava* L.) Extract. Adv. Nat. Sci. Nanosci. Nanotechnol., 9, 035006.

Sundari, J.J., Praba, P., Brightson, Y., Brightson Arul Jacob, Y., Vasantha, V., Shanmugaiah, V. (2017). Green Synthesis and Characterization of Zero Valent Iron Nanoparticles from the Leaf Extract of *Psidium guajava* Plant and Their Antibacterial Activity. Chem. Sci. Rev. Lett. 1244–1252.

Varadavenkatesan, T., Lyubchik, E., Pai, S., Pugazhendhi, A., Vinayagam, R., Selvaraj, R., (2019). Photocatalytic Degradation of Rhodamine B by Zinc Oxide Nanoparticles Synthesized Using the Leaf Extract of *Cyanometra ramiflora*. J. Photochem. Photobiol. B. Biol. 199, 111621.

Vasantharaj, S., Sathiyavimal, S., Senthilkumar, P., Lewis Oscar, F., & Pugazhendhi,A. (2019). Biosynthesis of Iron Oxide Nanoparticles Using Leaf Extract of *Ruellia tuberosa*: Antimicrobial Properties and Their Applications in Photocatalytic Degradation. J. Photochem. Photobiol. Biol. 192, 74–82.

Wanakai, S. I., Kareru, P. G., Makhanu, D. S., Madivoli, E. S., Maina, E. G., & Nyabola, A.O. (2019). Catalytic Degradation of Methylene Blue by Iron Nanoparticles Synthesized Using *Galinsoga parviflora*, *Conyza bonariensis* and *Bidens pilosa* Leaf Extracts. SN Applied Sciences. Springer Nature Journal. 1-1148.

Wang, Y., & Xia, Y. (2004). Bottom-up and Top-down Approaches to the Synthesis of Monodispersed Spherical Colloids of Low Melting point Metals. Nano Letters, 4(10), 2047-2050.

Wei, Y., Fang, Z., Zheng, L., Tan, L., & Tsang, E. P. (2016). Green synthesis of Fe Nanoparticles Using *Citrus maxima* Peels Aqueous Extracts.Mater Lett.185:384-6

Win, T.T., Khan, S., Bo, B., Zada, S. & Fu, P. (2021). Green Synthesis and Characterization of Fe_3O_4 Nanoparticles Using *Chlorella*-K01 Extract for Potential Enhancement of Plant Growth Stimulating and Antifungal Activity. Sci. Rep., 11, 21996.

Yu, J., Xu, D., Guan, H. N., Wang, C., Huang, L. K. (2016) Facile One-step Green Synthesis of Gold Nanoparticles Using *Citrus maxima* Aqueous Extracts and Its Catalytic Activity. Materials Letters 166, 110-112.

Zou, Z., Xi, W., Hu, Y., Nie, C., Zhou, Z. (2016). Antioxidant Activity of Citrus Fruits. Food Chemistry 196,885-896.